

4.10 Fault Interaction, Earthquake Stress Changes, and the Evolution of Seismicity

GCP King and MH Devès, Institut de Physique du Globe de Paris, Sorbonne Paris Cité, Univ. Paris Diderot, Paris, France

© 2015 Elsevier B.V. All rights reserved.

This chapter is a revision of the previous edition chapter by G C P King, Volume 4, pp. 225–255, © 2007, Elsevier B.V.

4.10.1	Introduction	243
4.10.2	Stress Interactions Between Faults in a Homogeneous Elastic Half-Space	244
4.10.2.1	Coulomb Failure	244
4.10.2.2	2D Case: Coulomb Stress on a Plane of Specified Orientation	245
4.10.2.3	2D Case: Change of Coulomb Stress on Optimally Orientated Faults	246
4.10.2.4	3D Case: Strike-Slip and Dip-Slip Conditions	248
4.10.2.5	Sensitivity to the Main-Shock Focal Mechanism	249
4.10.3	Examples of Coulomb Interactions	249
4.10.3.1	Coulomb Stress Changes and Aftershocks	249
4.10.3.2	Stress Changes Associated with the Landers Earthquake	251
4.10.3.3	Coulomb Stress Changes Preceding the Landers Rupture	251
4.10.3.4	Stress Changes Following the Landers Rupture but before the Big Bear Earthquake	251
4.10.3.5	Stress Changes Caused by the Landers, Big Bear, and Joshua Tree Ruptures	252
4.10.3.6	Interactions Between Large Earthquakes: Western Turkey and the Aegean	252
4.10.3.7	Interactions Between Very Large Earthquakes	256
4.10.3.8	Is It Better to Calculate Stress Transfer to Known Faults?	256
4.10.4	Introducing Time into the Failure Criterion	257
4.10.4.1	Time-Dependent Rock Failure	257
4.10.4.2	Rate- and State-Dependent Friction Equations	257
4.10.5	Loading Models and Lithospheric Properties	258
4.10.5.1	Elastic Half-Space Loading and Stress Relaxation Models	258
4.10.5.2	2D Plate-like Models	260
4.10.5.3	Inhomogeneous Lithospheric Models: The Effects of Voids or Fissures	260
4.10.5.4	Interactions Between Volcanic Eruptions and Earthquakes	260
4.10.5.5	Fluid Movement in Nonvolcanic Regions	260
4.10.5.6	The Distribution of Small Events Before Large Earthquakes	262
4.10.5.7	Stress Inhomogeneity Resulting from Displacement Boundary Conditions	262
4.10.6	Dynamic Triggering	269
4.10.7	Conclusions	269
Acknowledgment		269
References		269

4.10.1 Introduction

This chapter focuses on advances in our understanding of the Earth's lithosphere, over the last few decades – in particular, the way in which studies of earthquakes have added to our knowledge, by shedding light on how earthquakes interact one with another. There is a surprising lack of consensus about how the lithosphere behaves. We know that it is inhomogeneous at scales ranging from microns to tens or hundreds of kilometers, is porous, and is commonly anisotropic – remarks that apply with particular force to the continental lithosphere. Parts of the lithosphere are clearly brittle–elastic and generate earthquakes, but the greater part of the lithosphere is not seismogenic with a mechanical behavior that is poorly resolved. Even the brittle–elastic part behaves strangely when compared with the engineering materials that we normally come across. For example, before half the failure stress is reached in a laboratory sample, it has dilated dramatically. This effect has not been demonstrated

to occur at large scales, a disappointment to earthquake prediction attempts in the 1960s and 1970s, but serves to remind us that the behavior of rocks at one scale may be a poor guide to their behavior at another. Commonly, rock sample studies may be only a metaphor for the behavior at larger scales.

How does the nonseismogenic lithosphere behave? Visions vary on this. A persistent view has been that only the upper 10–20 km of the continental lithosphere, the upper crust, is seismogenic (i.e., brittle) and gives way to a lower crust that is viscous with no long-term strength. At greater depth, the Moho is reached and the upper mantle for perhaps 50 km is again strong and brittle.

This view is largely based on the results of laboratory tests conducted on homogeneous samples under very different strain rates, temperature conditions, and boundary conditions from those prevailing in the lithosphere. Nonetheless, the resulting model is mathematically and computationally tractable, and for geophysicists, it has provided a satisfying

explanation for a range of observations. Structural geologists have found the view difficult to accept. While not necessarily claiming that the entire lower crust and mantle are strong, a vision of highly localized shear zones (that only slip above a threshold stress) separated by strong, but deformable, blocks seems more appropriate to describe the structures observed in both active and deeply eroded mountain belts. Unlike the geophysicist's view, this vision is, in general, only mathematically tractable when greatly simplified to a system of rigid blocks separated by narrow deformation zones. These models can be quite complex when describing the mechanics of fold-thrust belts (e.g., Suppe, 1985). The two views have been described respectively as 'dynamic' because they incorporate stresses while the latter are described as kinematic because only geometry (including displacement vectors) is included. An intermediate view includes any time-dependent model based on stresses as dynamic. In this chapter, only phenomena for which momentum terms in their underlying equations cannot be ignored are termed dynamic (seismic waves and dynamic fault rupture).

The two views have been to a large extent supported by the different data sets that the 'geophysicists' and 'structural geologists' customarily study, but both sides can find some discomfort in their simplifications. For example, recent GPS results, best interpreted in terms of blocks, are difficult to reconcile with earlier views that the geodetic data supported distributed deformation. Structural geologists can be perturbed by evidence for massive ductile deformation in the lower crust and upper mantle. Not all geoscientists view the same data; geochemists and hydrologists observed evidence for massive migration of water in the lithosphere, and volcanologists have unequivocal evidence for the existence of massive regions of fluid rock, neither of which figure in the large-scale models outlined.

It was into this garden of confusion that the concepts of Coulomb stress interaction between earthquakes appeared in the 1980s. This met with astonishing success, while making the improbable simplification that the lithosphere is an homogeneous elastic half-space. Using this assumption, the stress on a second fault due to an earthquake on a first can be readily calculated. [Section 4.10.2](#) begins by outlining this simple mathematical formulation for Coulomb stress interaction. [Section 4.10.3](#) then provides examples of the method applied to both aftershock sequences and interactions between large events. Only aftershock sequences for strike-slip faults are illustrated since they offer the most straightforward examples. [Section 4.10.4](#) starts to consider modifications of the simple early theory by the introduction of time-dependent failure through the concept of rate and state friction.

Readers who are already familiar with the basic concepts outlined in [Sections 4.10.2–4.10.4](#) may wish to pass directly to later sections that consider unresolved problems and future perspectives in stress interaction studies. [Section 4.10.5](#) considers the effects of long-term loading and lithospheric inhomogeneities together with the effect of fluids including the interactions between faults and volcanoes. [Section 4.10.5](#) also describes why, in a medium subject to finite strain, the assumptions of infinitesimal strain or stress can never provide a complete description of fault interactions. Finally, the section discusses the accelerated seismic activity that appears over a wide region prior to major earthquakes. [Section 4.10.6](#) touches

on the question of dynamic triggering covered fully in [Chapter 4.11](#), and [Section 4.10.7](#) presents concluding remarks.

There are at least 250 papers that can be considered relevant to stress interactions, too many to refer to in any detail. Particular topics are therefore illustrated using a suitable example with no attempt to reference other work on the same topic. For more complete reference lists to earlier papers, the reader is referred to reviews Stein (1999), King and Cocco (2000), Freed (2005), and Steacy et al. (2005).

4.10.2 Stress Interactions Between Faults in a Homogeneous Elastic Half-Space

Faults are widely assumed to be well approximated as very narrow planes across which some components of displacement are discontinuous, while stress components across the plane are continuous. The system is driven by stress boundary conditions that determine the nature of the faulting: strike-slip, normal, or reverse. In turn, the faults exhibit a frictional behavior that determines the stress level at which they will slip to generate an earthquake. As discussed later, each of these assumptions can be challenged, but they allow a simple theoretical and computational framework to be developed on the basis of dislocation theory where static displacements, strains, and stresses can be computed by solving the elastostatic equation for a dislocation on a extended fault in an elastic, isotropic, and homogeneous medium. This solution yields the Volterra equation (Volterra, 1907),

$$u_m(x_i) = \frac{1}{F} \iint_{\Sigma} \Delta u_k(\xi_i) T_{kl}^m(\xi_i, x_i) n_l(\xi_i) d\Sigma(\xi_i)$$

where F is the magnitude of a volume point force applied at $\vec{\xi}$ in the direction m . n_k are the components of the unit vector normal to the components of the unit vector normal to the surface element $d\Sigma$. The static displacement $u_m(x_i)$ is computed as a function of the dislocation $\Delta u_k(\xi_i)$ and the static traction $T_{kl}^m(\xi_i, x_i)$ on the fault plane Σ . The previous equation becomes

$$u_m(x_i) = \frac{1}{F} \iint_{\Sigma} \Delta u_k \left[\lambda \delta_{kl} \frac{\partial U_m^n}{\partial \xi_n} + \left(\frac{\partial U_m^k}{\partial \xi_l} + \frac{\partial U_m^l}{\partial \xi_k} \right) \right] n_l d\Sigma$$

where the summation convention applies (e.g., Aki and Richards, 1980); computation of the static displacement requires knowledge of the fault geometry, the slip distribution, and the strain nuclei (Mindlin, 1936) $U_m^k(\xi_i, x_i)$ (i.e., the static Green's functions). Using these solutions and Hooke's law analytic expressions for the static displacement, strain and stress fields caused by a finite rectangular fault within an elastic half-space have been derived (Okada, 1985).

4.10.2.1 Coulomb Failure

A number of criteria can be used to characterize failure in rocks of which the Coulomb failure criterion is widely used (e.g., Scholz, 1998). It requires that both the shear and normal stress on a preexisting or an incipient fault plane satisfy conditions analogous to those of friction on a preexisting surface.

Failure initiates and spreads on the plane when the Coulomb stress C_f sometimes referred to as the Coulomb failure function (CFF) exceeds a specific value

$$C_f = \tau_\beta + \mu(\sigma_\beta + p) \quad [1]$$

where τ_β is the shear stress on the failure plane, σ_β is the normal stress (positive for extension), p is the pore fluid pressure, and μ the coefficient of friction. The value of τ_β must always be positive in this expression. However, the processes of resolving shear stress onto an assigned plane may give positive or negative values. The difference in sign of τ_β indicates whether the potential for slip on the plane is right or left lateral.

If the failure plane is orientated at β to the σ_1 axis (see [Figure 1](#)), we can express, under plane-stress conditions, the normal stress applied to the plane in terms of the principal stresses:

$$\sigma_\beta = \frac{1}{2}(\sigma_1 + \sigma_3) - \frac{1}{2}(\sigma_1 - \sigma_3) \cos 2\beta \quad [2]$$

Two expressions are required for shear stress, the one giving positive values being chosen. One is for left-lateral and the other for right-lateral shear stress:

$$\begin{aligned} \tau_\beta^L &= \frac{1}{2}(\sigma_1 - \sigma_3) \sin 2\beta \\ \tau_\beta^R &= -\frac{1}{2}(\sigma_1 - \sigma_3) \sin 2\beta \end{aligned} \quad [3]$$

where σ_1 is the greatest principal stress and σ_3 is the least principal stress. For left- and right-lateral Coulomb stresses, eqn [1] then becomes:

$$C_f = \frac{1}{2}(\sigma_1 - \sigma_3)(\sin 2\beta - \mu \cos 2\beta) - \frac{1}{2}\mu(\sigma_1 + \sigma_3) + \mu p \quad [4]$$

where the sign of the shear stress is taken to indicate left- or right-lateral motion. By differentiating the last eqn [4] as a function of β , one finds that the maximum Coulomb stress C_f^{\max} occurs for two angles when

$$\tan 2\beta = -\mu \quad [5]$$

Pore fluid pressure modifies the effective normal stress across the failure plane as shown in eqn [1]. When rock stress is changed more rapidly than fluid pressure can change through flow, pore fluid pressure, p , can be related to confining stress in the rock by Skempton's coefficient B ($p = -B\sigma_{kk}/3$), where B varies between 0 and 1. Equation [1] and subsequent

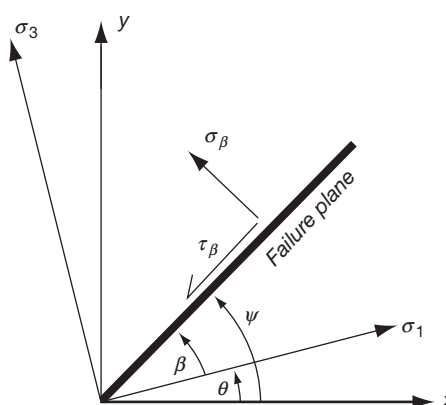


Figure 1 The axis system used for calculations of Coulomb stresses. Extension and left-lateral motion on the failure plane are assumed to be positive. The sign of τ_β is reversed for calculations of right-lateral Coulomb failure on specified planes.

expressions (such as eqn [4]) can therefore be rewritten on the assumption that σ_β represents the confining stress as well as the normal stress on the plane ($p = -B\sigma_\beta$)

$$C_f = \tau_\beta + \mu' \sigma_\beta \quad [6]$$

where the effective coefficient of friction is defined by $\mu' = \mu(1 - B)$. Although useful, it must be remembered that the expression is an approximation since the normal stress across a plane needs not be so simply related to confining stress (e.g., [Cocco and Rice, 2002](#)). Further problems associated with fluid flow are discussed later.

The failure condition is inherently two-dimensional (2D) with the intermediate stress σ_2 playing no part. Thus, the underlying physics can be illustrated in 2D. To generalize the mathematics to 3D, it is only necessary to determine the orientation of the plane of greatest and least principal stresses in the appropriate coordinate system and to apply the failure conditions in that plane.

4.10.2.2 2D Case: Coulomb Stress on a Plane of Specified Orientation

In a system where the x - and y -axes and fault displacements are horizontal and fault planes are vertical (containing the z direction), stress on a plane at an angle ψ from the x -axis (see [Figure 2](#)) resulting from a general stress field of any origin is given by:

$$\begin{aligned} \sigma_{11} &= \sigma_{xx} \cos^2 \psi + 2\sigma_{xy} \sin \psi \cos \psi + \sigma_{yy} \sin^2 \psi \\ \sigma_{33} &= \sigma_{xx} \sin^2 \psi - 2\sigma_{xy} \sin \psi \cos \psi + \sigma_{yy} \cos^2 \psi \\ \tau_{13} &= \frac{1}{2}(\sigma_{yy} - \sigma_{xx}) \sin 2\psi + \tau_{xy} \cos 2\psi \end{aligned} \quad [7]$$

where these relations hold for a left-lateral mechanism ($\tau_{13} = \tau_{13}^L$) and similar expressions can be derived for a right-lateral mechanism (as stated in eqn [3]). The Coulomb stress for left-lateral C_f^L and right-lateral C_f^R motion on planes orientated at ψ with respect to the x -axis can now be written in the following way:

$$C_f^L = \tau_{13}^L + \mu' \sigma_{33} \quad [8a]$$

$$C_f^R = \tau_{13}^R + \mu' \sigma_{33} \quad [8b]$$

Equation [8b] is illustrated in [Figure 2\(a\)](#) using a dislocation (earthquake fault) source. An elliptical slip distribution is imposed on the (master) fault in a uniform, stress-free, elastic medium. The contributions of the shear and normal components to the failure condition and the resulting Coulomb stresses for infinitesimal faults parallel to the master fault (commonly referred to as target faults) are shown in separate panels. Such a calculation represents the Coulomb stress on these planes resulting from slip on the master fault (i.e., the figure shows a map of stress changes) and is independent of any knowledge of the prevailing regional stresses or any pre-existing stress fields from other events. The signs in the calculation are chosen such that a positive Coulomb stress indicates a tendency for slip in the same right-lateral sense as the fault of interest. Negative Coulomb stresses indicate a reduction of this tendency. It is important to appreciate that because τ_{13} changes sign between eqns [8a] and [8b], a negative Coulomb stress for right-lateral fault motion is not the same as a tendency for left-lateral slip.

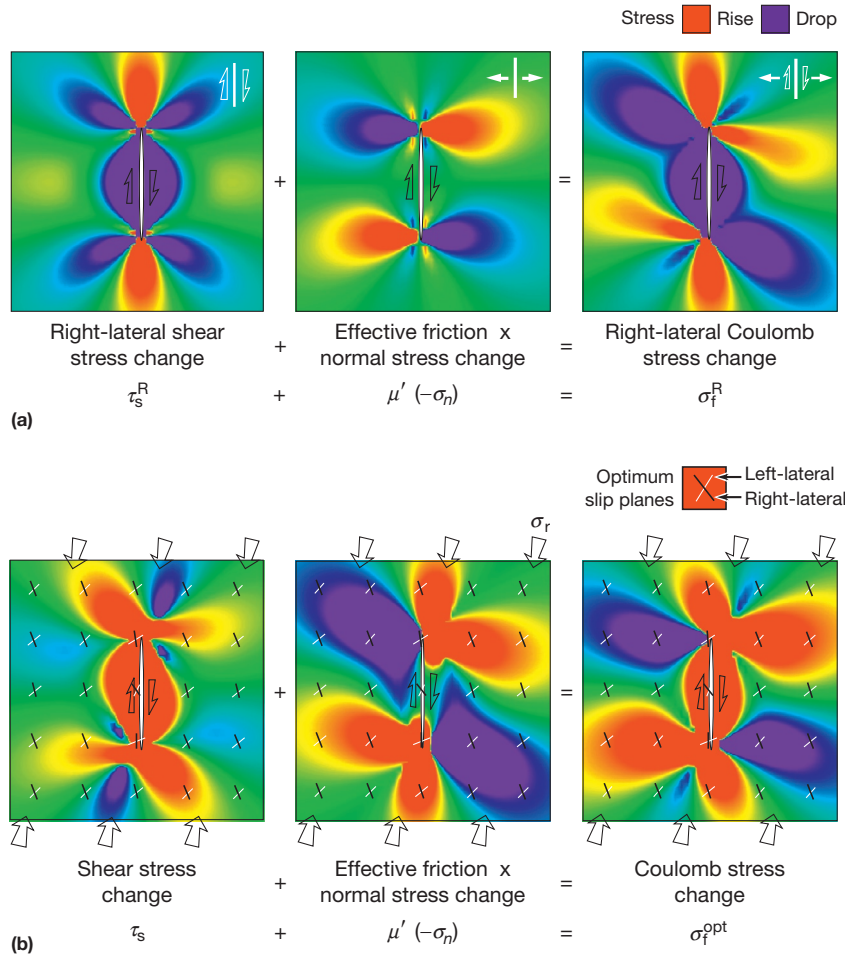


Figure 2 Map view of Coulomb stress changes caused by a right lateral strike-slip fault in plane strain. (a) Coseismic shear, normal, and Coulomb stress changes for right-lateral fault parallel to the master fault. (b) Shear, normal, and Coulomb stress changes on optimally oriented faults (black and white segments) with respect to a regional stress characterized by a N7°E (open arrows) compression of 100 bar. The slip distribution on the fault plane is uniform, but it tapers at the fault ends. The effective friction coefficient μ' is taken to be 0.4. Redrawn after King GCP, et al. (1994b). Static stress changes and the triggering of earthquakes. *Bulletin of the Seismological Society of America* 84: 935–953.

The distribution of increases and decreases of Coulomb stress shows features common to all subsequent figures. Lobes of increased shear stress appear at the fault ends, corresponding to the stress concentrations that tend to extend the fault. Off-fault lobes also appear on either side of the fault, separated from the fault by a region where the Coulomb stresses have not been increased. If the master fault was infinitesimal in length and thus behaving as a point source, all four lobes would be equal in amplitude to the fault-end lobes at all distances. The normal stress field is similar to the more familiar dilatational field with maxima and minima distributed antisymmetrically across the fault, but we consider only the component of tension normal to the fault. The influence of the normal stress on the Coulomb stress distribution is to reduce the symmetry of the final distribution and to increase the tendency for off-fault failure.

4.10.2.3 2D Case: Change of Coulomb Stress on Optimally Orientated Faults

The calculation in the previous section is general and need not be due to an earthquake. If a stress or stress change is known,

then the Coulomb stress or stress change can be calculated on any plane. The more general case where a change of stress, such as that due to an earthquake, is imposed on a preexisting stress field can be calculated. The failure planes are not specified a priori, but are computed accounting for the interaction between the two fields. Optimal planes are regarded as those simultaneously favored by tectonic loading and the stress induced by the motion on the master fault. Here, we define such planes in terms of uniformly varying stress fields. The optimum directions are determined by the stress change due to that earthquake $\sigma_{ij}^q (= \Delta\sigma_{ij})$ and by existing regional stresses σ_{ij}^r that gives a total stress σ_{ij}^t

$$\sigma_{ij}^t = \sigma_{ij}^r + \sigma_{ij}^q \quad [9]$$

The orientation of the principal axes resulting from the total stress is therefore derived using

$$\theta = \frac{1}{2} \tan^{-1} \left(\frac{2\sigma_{xy}^t}{\sigma_{xx}^t - \sigma_{yy}^t} \right) \quad [10]$$

where θ is the orientation of one principal axis to the x -axis as shown in Figure 1 and the other is at $\theta \pm 90^\circ$. From these two

directions, the angle of greatest compression θ_1 must be chosen. The optimum failure angle ψ_0 is then given by $\theta_1 \pm \beta$ where one plane is left and the other right lateral with the sign of shear stress being chosen appropriately. Whereas the optimum planes are determined from σ_{ij}^t , the normal and shear stress changes on these planes are determined only by the earthquake stress changes σ_{ij}^q . Thus, the changes in stress on the optimum planes become

$$\begin{aligned}\sigma_{33} &= \sigma_{xx}^q \sin^2 \psi_0 - 2\sigma_{xy}^q \sin \psi_0 \cos \psi_0 + \sigma_{yy}^q \cos^2 \psi_0 \\ \tau_{13} &= \frac{1}{2} (\sigma_{yy}^q - \sigma_{xx}^q) \sin 2\psi_0 + \tau_{xy}^q \cos 2\psi_0\end{aligned}\quad [11]$$

and the Coulomb stress changes on the planes are equal and given by

$$C_f^{\text{opt}} = \tau_{13} + \mu' \sigma_{33} \quad [12]$$

The two optimum planes correspond to left- and right-lateral shear. The Coulomb stress change is the same on both so that the Coulomb stress is the same whether calculated for left- or right-lateral planes in expression [12]. It is important to emphasize that we calculate the change of Coulomb stress on planes that are optimum after the earthquake with the optimum orientations being calculated from the earthquake stress field plus the regional stress field. The Coulomb stress changes caused by the earthquake stress changes are then resolved onto these planes. Where earthquake stresses are large, they can rotate the principal axes.

The results of a calculation to find optimum orientations and magnitudes of Coulomb stress changes are shown in Figure 2(b). The slip on the master fault is the same as before (Figure 2(a)). A uniform 100-bar compressional stress is introduced with the orientation shown. White lines indicate

optimum left-lateral orientations and black lines, right-lateral orientations. The shear and normal stress contributions to the Coulomb stress change are again shown in separate panels.

It can be seen from expression [9] that only the deviatoric part of the regional stress determines the orientation of principal axes and hence the optimum stress orientations. Thus, it is sufficient to apply the regional stress as a simple uniaxial compression or extension. This assumes, however, the intermediate principal stress is vertical and thus a 2D description is complete. In general, this is not true since the relative magnitudes of the principal stresses control the focal mechanisms that not be strike-slip.

The relative amplitude of the regional stress to the earthquake stress drop ($\Delta\tau$) might be expected to have an effect. This is explored for the strike-slip case in Figure 3, which shows the Coulomb stress change C_f^{opt} on optimally orientated right-lateral planes in which the regional field is equal to the stress drop $\Delta\tau$ (left panel) and ten times $\Delta\tau$ (right panel). These examples span likely conditions. It is evident that, except close to the master fault, the orientations of the optimal planes and Coulomb stress changes on these planes are little altered. The optimal orientations are essentially fixed by the regional stress except very close to the fault where the stress change caused by slip on the master fault is comparable to the regional stress. Thus, for stress drops similar in amplitude to the regional stress, Coulomb stress changes close to the fault are always positive. (For a regional stress of zero, they are positive everywhere.)

The effects of varying the orientation of regional stresses and changing the coefficient of friction μ' are shown in Figure 4. Possible changes of regional stress orientation are limited since the main fault must move as a result of the

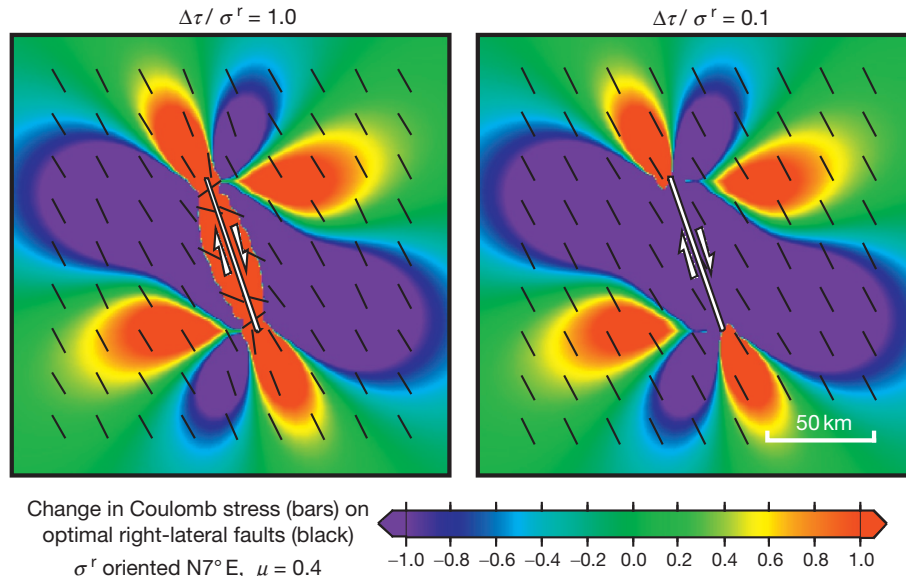


Figure 3 Coulomb stress changes for different magnitudes of the regional stress. The left panel shows the Coulomb stress changes for an earthquake stress drop similar in amplitude to the deviatoric regional stress, while the right panel shows the same calculations for a larger (ten times) regional stress amplitude. The former case represents the stress perturbation caused by an earthquake relieving all of the regional stress. In this case, the resulting optimally oriented planes (black segments) for failure rotate from the direction predicted by the regional deviatoric stress near the causative fault, where the induced coseismic stress is larger. Far away from the fault (left panel), where the regional stress amplitude is larger than the induced one, the optimally oriented planes follow the regional stress (see also the right panel). Redrawn after King GCP, et al. (1994b) Static stress changes and the triggering of earthquakes. *Bulletin of the Seismological Society of America* 84: 935–953.

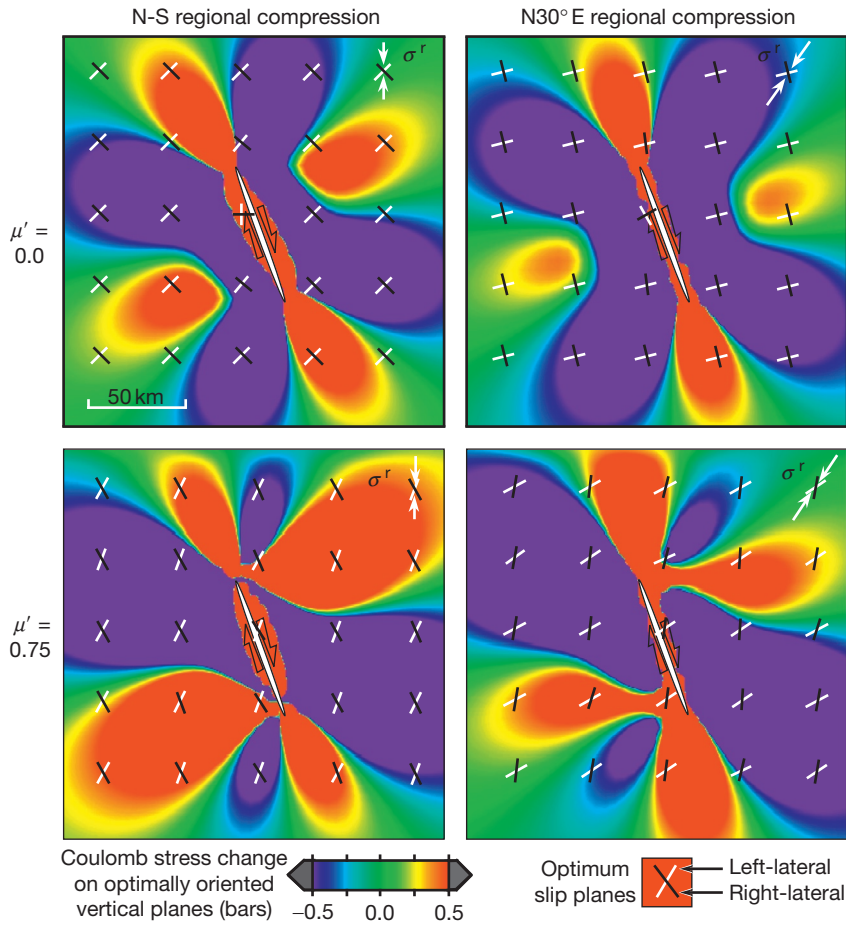


Figure 4 Coulomb stress changes for different orientations of the regional deviatoric stress (left and right panels) and for different values of the effective friction coefficient (upper and bottom panels). Both configurations of the regional stress field refer to horizontal s_1 and s_3 directions. Stress changes are caused by a 70 km long and 12.5 km wide vertical right-lateral fault with 5 m of tapered slip. The regional stress amplitude is 100 bar as in [Figure 3](#). The regional stress orientation controls the size of the off-fault to fault-end lobes. The effective friction coefficient controls the internal angle between right- and left-lateral slip planes. Redrawn after King GCP, et al. (1994b) Static stress changes and the triggering of earthquakes. *Bulletin of the Seismological Society of America* 84: 935–953.

regional stress; the 30° range covers the likely range. Similarly, values of friction between 0.0 and 0.75 span the range of plausible values. All of the panels show the same general features, fault-end and off-fault Coulomb stress lobes. Thus, modeling is most sensitive to the regional stress direction, almost insensitive to the regional stress amplitude and modestly sensitive to the coefficient of effective friction. In other words, while the relative magnitude of the regional stress with respect to the earthquake stress drop controls the changes in the orientations of the optimal planes close to the master fault (as shown in [Figure 4](#)), the orientation of the regional stress is the most important factor controlling the orientations of the optimal planes for failure far away from the master fault.

4.10.2.4 3D Case: Strike-Slip and Dip-Slip Conditions

The application to vertical strike-slip faults is easy because a 2D problem (plane-stress configuration) can be solved with the vertical components of the regional stress tensor neglected. However, the application to dip-slip faults requires the solution of a 3D problem where the ratio between vertical and

horizontal components of regional stress tensor must be known. This means that, while in the foregoing discussion, we have assumed that only strike-slip vertical faults are present and thus stress components σ_{zz} , σ_{xz} , σ_{yz} could be neglected, in a more general configuration, these stress components cannot be ignored.

If the regional stress components are known, the total stress can be computed through eqn [9], which is used to find the orientation and magnitude of the principal stresses. We can therefore calculate the orientation of the plane containing σ_1 and σ_3 , and hence, the optimum orientations of slip planes where the change of Coulomb failure stress will be found. The calculation is straightforward and an example is shown in [Figure 5](#). If we take horizontal stresses similar in amplitude to those employed before, we can examine the change of mechanism as the vertical stress is changed. The horizontal stresses are chosen to be 200 (EW) and 400 bar (NS). For [Figure 5\(a\)](#), the vertical stress is 100 bar; in [Figure 5\(b\)](#), the vertical stress is 300 bar; and in [Figure 5\(c\)](#), the vertical stress is 500 bar. The predominant mechanisms are reverse faulting in [Figure 5\(a\)](#), strike-slip faulting in [Figure 5\(b\)](#), and normal

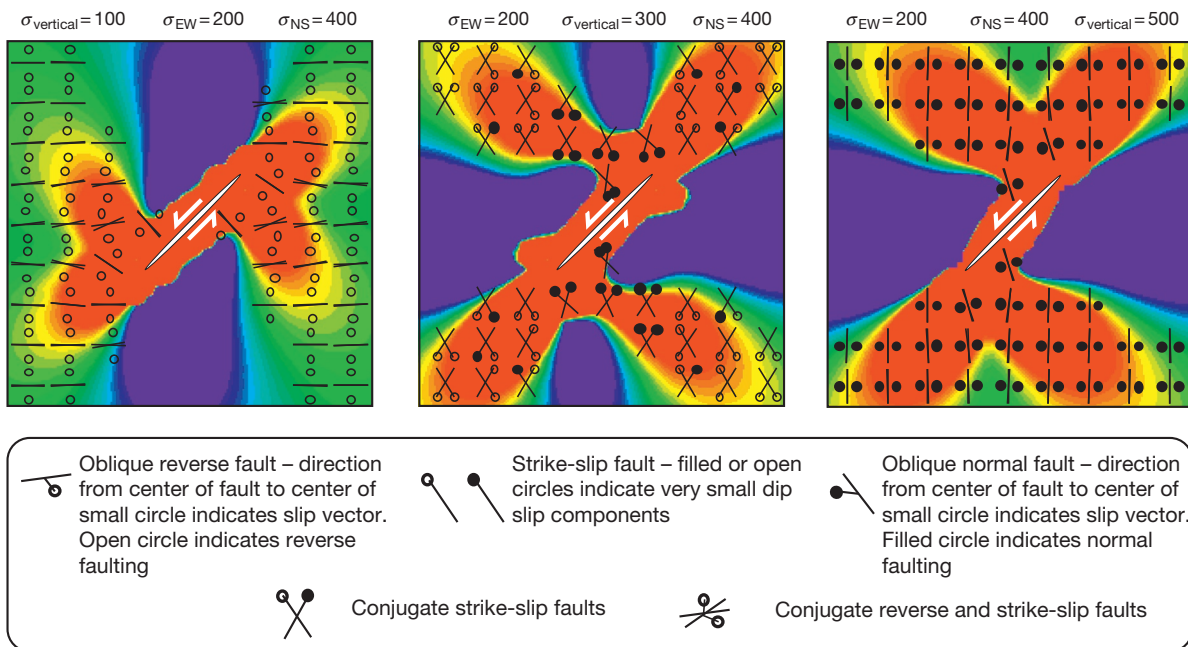


Figure 5 Coulomb stress changes and optimally oriented planes for different orientations of the regional stress field. The vertical stress coincides with the least principal stress (100 bar) in the left panel, with the intermediate principal stress (300 bar) in the middle panel, and with the greatest principal stress (500 bar) in the right panel. Therefore, the predicted faulting mechanisms on optimally oriented planes are strike-slip in the middle panel and inverse or normal in the left and right panels, respectively.

faulting in [Figure 5\(c\)](#)). If the vertical stresses are attributed to overburden pressure, then the figures correspond to depths of 300, 900, and 1500 m, respectively. This is clearly incorrect. Events do not occur at such shallow depths nor are systematic changes of focal mechanism with depth observed. It would seem that a confining pressure that increases with depth must be added to the horizontal stress such that the differential stresses remain similar. It is clear, however, that the mechanisms are sensitive to small variations in the stresses chosen; thus, to correctly predict mechanisms from stresses, the stress regime must be known with precision. Direct measurements of stress throughout the seismogenic zone are never available; thus, predicting mechanisms from stress must be indirect. In practice, the most useful stress information comes from some sort of average of the stress orientation required to generate the observed focal mechanisms in the region. As discussed in [Section 4.10.3.8](#), we explain that calculation of stress changes on individual fault planes from determined focal mechanisms might be preferred.

4.10.2.5 Sensitivity to the Main-Shock Focal Mechanism

The last section showed that the Coulomb distribution can be sensitive to incorrect assumptions about regional stress since this can cause target fault focal mechanisms to be incorrectly predicted. While nearby events are clearly sensitive to all of the details of the rupture process, this is not the case some distance from the fault. As shown in [Section 4.10.2.3](#), the orientation of the regional stress is the most important factor controlling the orientations of the optimal planes for failure far away from the master fault. This is particularly important for studying fault interaction between large magnitude earthquakes. Completely

incorrect focal mechanisms clearly result in incorrect results. Errors in dip (within an acceptable range) are much less serious. [Figure 6\(a\)](#) shows the distribution for a 45° dipping normal fault, and [Figure 6\(b\)](#) shows the distribution for a vertical dike with the same opening displacement as the horizontal slip vector of the dip-slip fault. Except at distances comparable to the source dimensions, the two distributions are identical. This illustrates that, except close to a dip-slip fault, the fault dip is not important. In general, except in the near field (or at distances of few fault lengths), a double couple point source with the appropriate seismic moment is all that is needed.

While large errors in the strike of the focal planes are serious, small errors only result in (an approximately) commensurate rotation of the Coulomb stress distribution. This is shown in [Figure 6\(c\)](#). It can be remarked at this point that it is much harder to evaluate the fault parameters close to dip-slip faults making aftershock studies of such events more difficult than for strike-slip events. We therefore choose to illustrate aftershock studies for strike-slip events and large event interactions for dip-slip events.

4.10.3 Examples of Coulomb Interactions

4.10.3.1 Coulomb Stress Changes and Aftershocks

The methods outlined earlier can be applied to aftershock distributions. [Figure 7](#) shows the 1979 Homestead Valley aftershock sequence. There are four lobes of Coulomb stress rise and four lobes of Coulomb stress drop. The lobes at the ends of the fault extend into the fault zone, while the off-fault lobes are separated from the fault over most of its length by a

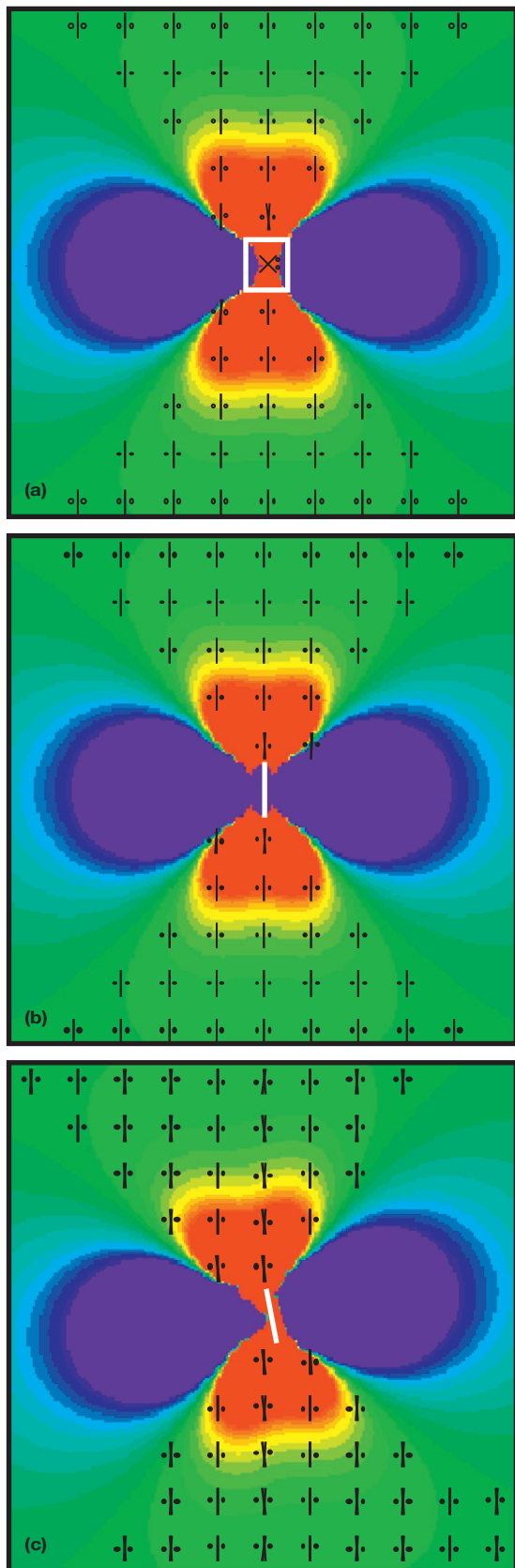


Figure 6 Coulomb stress changes caused by a 45° dipping normal fault (a), a vertical dike with the same opening displacement as the horizontal

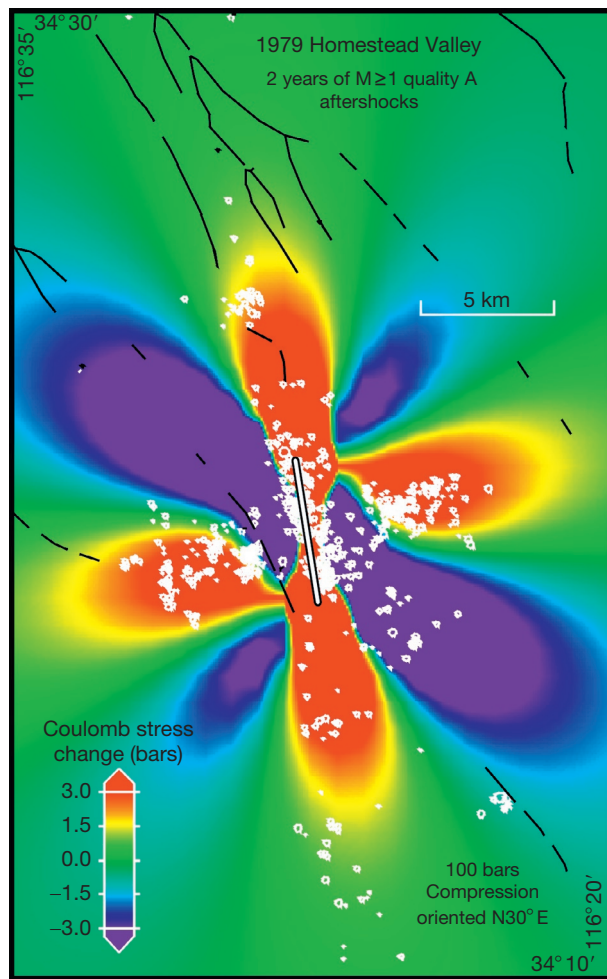


Figure 7 Coulomb stress changes caused by the 15 March 1979 Homestead Valley earthquake sequence (redrawn after King GCP, et al. (1994b). Static stress changes and the triggering of earthquakes. *Bulletin of the Seismological Society of America* 84: 935–953) and aftershock distribution (the same shown in Figure 1). The calculations are carried out in a half-space with the values of Coulomb stress plotted in the figures being calculated at half the depth to which the faults extend. The fault is 5.5 km long and 6 km wide and slip is 0.5 m and it is tapered at the fault ends.

zone where the Coulomb stress is reduced. The distributions of aftershocks are consistent with these patterns. Many events are associated with increases of Coulomb stress of < 1 bar, while reductions of the same amount apparently suppress them. Relatively few events fall in the regions of lowered Coulomb stress, and the clusters of off-fault aftershocks are separated from the fault itself by a region of diminished activity. The distributions of Coulomb stresses can be modified as described earlier by adjusting the regional stress direction and

slip vector of the dip-slip fault (b), and a 45° dipping normal fault with a different strike (c). Except at distances comparable to the source dimensions, the two distributions are identical, suggesting that, except close to a dip-slip fault, the fault dip is less important than fault strike; in this latter case, errors only result in an approximately commensurate rotation of the Coulomb stress distribution. Symbols as in Figure 5.

changing μ . However, any improvements in the correlation between stress changes and aftershock occurrence are modest. Consequently, we have chosen to show examples with an average μ' of 0.4. Whatever values we adopt, we find that the best correlations of Coulomb stress change to aftershock distribution are at distances greater than a few kilometers from the fault. Closer to the fault, unknown details of fault geometry and slip distribution influence the stress changes. Correlation between aftershock distribution and Coulomb stress changes on a vertical cross section can also be observed and are discussed by King et al. (1994b).

4.10.3.2 Stress Changes Associated with the Landers Earthquake

Although stress interactions had been previously observed for other events, the clear correlations associated with the Landers earthquake suggested to the scientific community that Coulomb calculations might indeed prove an effective method of relating large events with each other and relating large events to their aftershock sequences. The Landers earthquake and associated events remain the best example for illustrating the techniques and we reproduce here the modeling processes following King et al. (1994b). Since the main events were strike-slip (except for Cedar Mountain), the calculations are essentially 2D and an 'effective' regional stress is easy to establish since only the deviatoric part in the horizontal plane is needed.

4.10.3.3 Coulomb Stress Changes Preceding the Landers Rupture

Figure 8 shows the Coulomb stress changes caused by the four $M > 5$ earthquakes within 50 km of the epicenter that preceded the Landers earthquake. The Coulomb stresses are due to the 1975 $M_L = 5.2$ Galway Lake, 1979 $M_L = 5.2$ Homestead Valley, 1986 $M_L = 6.0$ North Palm Springs, and 1992 $M_L = 6.1$ Joshua Tree earthquakes. These progressively increased Coulomb stresses by about 1 bar at the future Landers epicenter. Together, they also produced a narrow zone of Coulomb stress increase of 0.7–1.0 bar, which the future 70 km long Landers rupture followed for 70% of its length. The Landers fault is also nearly optimally oriented for most of its length. It is noteworthy that the three largest events are roughly equidistant from the future Landers epicenter: the right-lateral Homestead Valley and Joshua Tree events enhanced stress as a result of the lobes beyond the ends of their ruptures, whereas the North Palm Springs event enhanced rupture as a result of an off-fault lobe. Increasing the effective friction μ' from 0.4 (Figure 8) to 0.75 slightly enhances the effects and dropping the friction to zero reduces them.

4.10.3.4 Stress Changes Following the Landers Rupture but before the Big Bear Earthquake

Unlike the earthquake sources modeled so far, which are approximated by an elliptical slip distribution on a single plane, there is more information about the $M=7.4$ Laders source that following the rupture is modeled with 13 fault

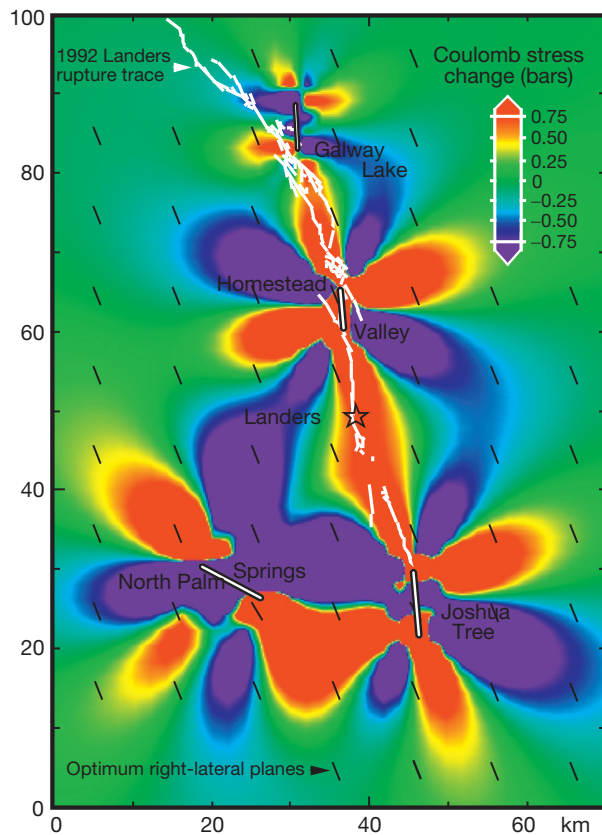


Figure 8 Coulomb stress changes caused by the four earthquakes that preceded the 1992 Landers main shock within 50 km of the epicenter. The source parameters used in this calculation are listed in King et al. (1994b). These events raised the stress at the future Landers epicenter and on most (70%) of the Landers rupture.

segments to produce a slip distribution that is consistent with surface fault mapping, geodetic data, radar data, and the modeling of seismic data.

The stress changes caused by the Landers event are shown in Figure 9. The largest lobe of increased Coulomb stress is centered on the epicenter of the future $M_L = 6.5$ Big Bear event, where stresses were raised 2–3 bar. The Big Bear earthquake was apparently initiated by this stress rise 3 h 26 min after the Landers main shock. The Coulomb stress change at the epicenter is greatest for high effective friction but remains more than 1.5 bar for $\mu' = 0$. There is no surface rupture or Quaternary fault trace associated with the Big Bear earthquake. Judging from its epicenter and focal mechanism, the plane that apparently ruptured was optimally aligned for left-lateral failure, with the rupture apparently propagating northeast and terminating where the Landers stress change became negative.

In addition to calculating the stress changes caused by the Landers rupture, an estimate can be made of the slip on the Big Bear fault needed to relieve the shear stress imposed by the Landers rupture. This is achieved by allowing the Big Bear rupture plane to slip freely as in the stress field caused by the Landers rupture. The potential slip along the Big Bear fault is 60 mm (left lateral), about 5–10% of the estimated slip that

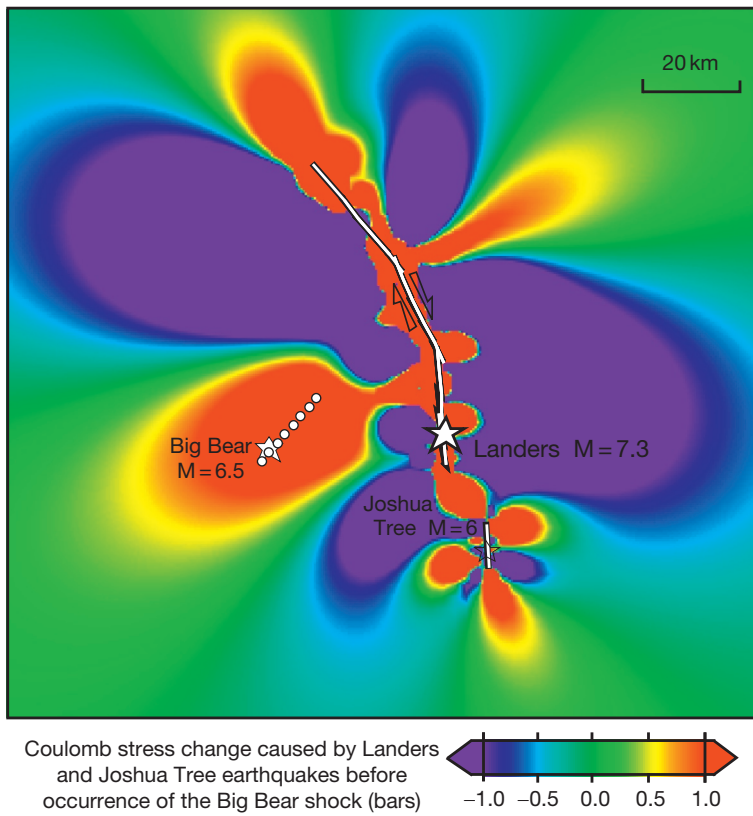


Figure 9 Coulomb stress changes caused by the 1992 Joshua Tree and Landers earthquakes. The location of the Big Bear aftershock and its faulting mechanism are consistent with the induced coseismic stress field. Redrawn after King GCP, et al. (1994b) Static stress changes and the triggering of earthquakes. *Bulletin of the Seismological Society of America* 84: 935–953.

occurred. These calculations suggest that the Big Bear slip needed to relieve the stress imposed by Landers was a significant fraction of the total slip that later occurred. Thus, from consideration of the stress changes and the kinematic response to those changes, it has been considered reasonable to propose that stresses from the Landers event played a major role in triggering the Big Bear shock.

4.10.3.5 Stress Changes Caused by the Landers, Big Bear, and Joshua Tree Ruptures

The Big Bear earthquake was the largest of more than 20 000 aftershocks located after the Landers earthquake, large enough to result in significant stress redistribution at the southwestern part of the Landers rupture zone. Consequently, the distribution of later events cannot be examined without considering its effect. Although smaller, a similar argument can be applied to the Joshua Tree event, whose aftershock sequence was not complete at the time of the Landers rupture. In [Figure 10](#), the combined Coulomb stress changes for the Joshua Tree, Landers, and Big Bear earthquakes are plotted. This distribution is shown together with all well-located $M_L \geq 1$ events that occurred during the following 25 days.

Most $M_L > 1$ aftershocks occur in regions where the failure stress is calculated to have increased by ≥ 0.1 bar, and few events are found where the stress is predicted to have dropped ([Figure 10](#)). Even when all seismicity within 5 km of the

Landers, Big Bear, and Joshua Tree faults is excluded, more than 75% of the aftershocks occur where the stress is predicted to have risen by > 0.3 bar. In contrast, $< 25\%$ of the aftershocks occur where the stress dropped by > 0.3 bar.

4.10.3.6 Interactions Between Large Earthquakes: Western Turkey and the Aegean

The Landers earthquake sequence suggests that a series of smaller events that preceded the Landers earthquake prepared a region of slightly elevated stress along much of the fault that the main event then followed ([Figure 8](#)). It is also clear that the stresses created by the main event largely controlled the aftershock distribution, including the location of the large ‘Big Bear’ aftershock. A number of studies have shown that large events appear to interact over large areas (see reviews quoted in the introduction for more detailed reference lists). Here, we illustrate the effect taking an example from Turkey and the western Aegean. Since 1912, 29 events ($M_s \geq 6.0$) have occurred in the region shown in [Figure 11](#). The area in the west is of particular interest because the events, unlike the sequence that occurred further east on the North Anatolian Fault events, do not lie along a single fault requiring to result from both on- and off-fault Coulomb stress changes. The events are predominantly strike-slip and normal faulting, but some reverse faulting occurs. The later events have reliable focal mechanisms and seismic moments controlled by waveform modeling. Earlier

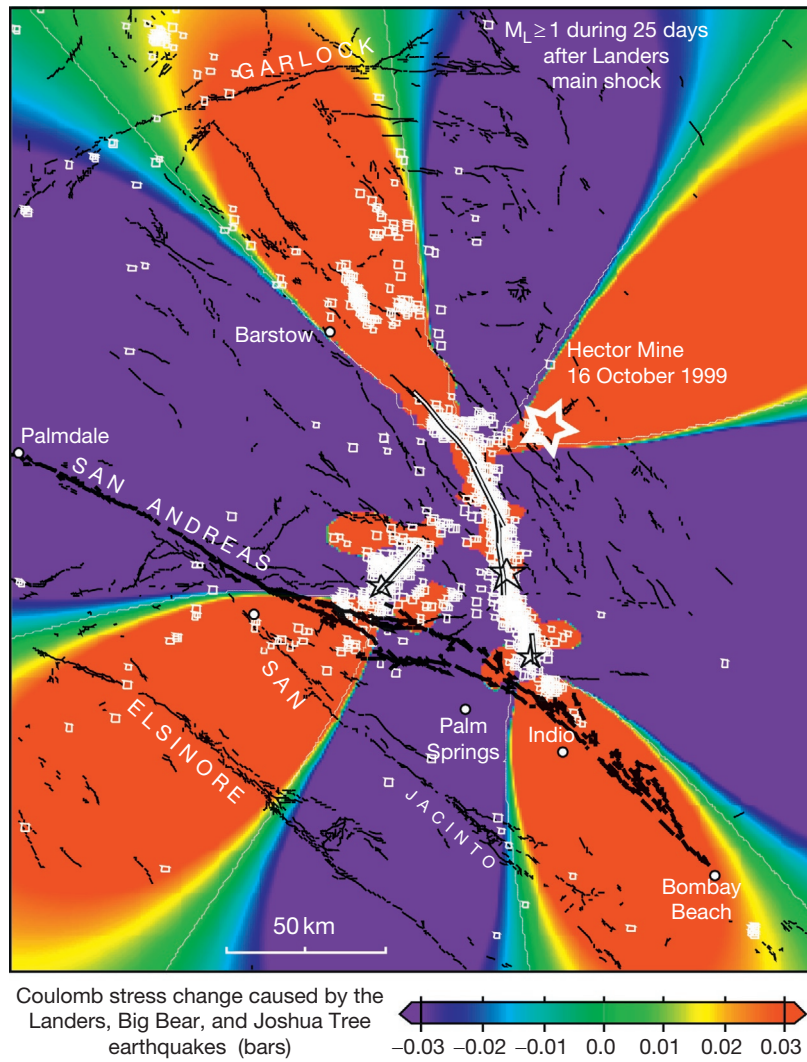


Figure 10 Coulomb stress changes caused by the Joshua Tree, Landers, and Big Bear earthquakes mapped at a depth of 6.25 km (halfway down the fault) and ($M \geq 1$) aftershock distribution during the 25 days following the Landers main shock. Source parameters are those used by King et al. (1994a,b). The location (open star) and the surface rupture (solid black line) of the $M 7.1$, 1999, Hector Mine earthquake epicenter are shown on the map. The Coulomb stress changes are plotted with a reduced amplitude (color) scale with respect to those of the previous figures. Redrawn after King GCP, et al. (1994b) Static stress changes and the triggering of earthquakes. *Bulletin of the Seismological Society of America* 84: 935–953.

events do not, but a combination of geologic information to identify the faults involved together with damage information closely controls the possible mechanisms. Details of the mechanism information can be found in Nalbant et al. (1998) from which the examples presented here are abstracted. That paper splits the time period into nine intervals such that all interactions can be seen. Here, we only show three example time windows: they are 1912–44 (Figure 12(a)), 1912–67 (Figure 12(b)), and 1912–96 (Figure 12(c)). These are insufficient to demonstrate all the interactions that require the original figures to be examined but allow the reader to gain an impression of the size of the events and the distances between them. The results can be summarized as follows: out of 29 events, 16 (1935, 1939, 1944.1, 1953, 1957, 1964, 1967.2, 1968, 1969, 1970, 1975, 1978, 1981.1, 1981.2, 1982, and 1983) occurred in regions where stress was increased by more than 0.1 bar. If less certain information about earlier

events is used and smaller stress increases are presumed to be significant, then 23 of the 29 events appear to have responded to Coulomb stress interactions. Stein et al. (1997) examined interactions between ten events extending to the east of the region shown in Figure 10(c). Of these, all but one (eight out of ten) occurred in regions of substantially enhanced Coulomb stress. For the East Anatolian Fault, Nalbant et al. (2002) (Figure 10(c)) had shown that nine out of ten events ($M > 6.7$) occurred in regions of enhanced Coulomb stress. Taken together with the Nalbant et al. (1998) work, 33 out of 49 events since 1912 along the North and East Anatolian fault and the Aegean system show clear Coulomb interactions. If less certain information is included, then this rises to 41 out of 49. Of great importance, not one substantial event occurred in the mauve regions where Coulomb stress was reduced. Such regions have been described as stress shadows (Harris, 1998; Toda et al., 2012) and with some reservations discussed later

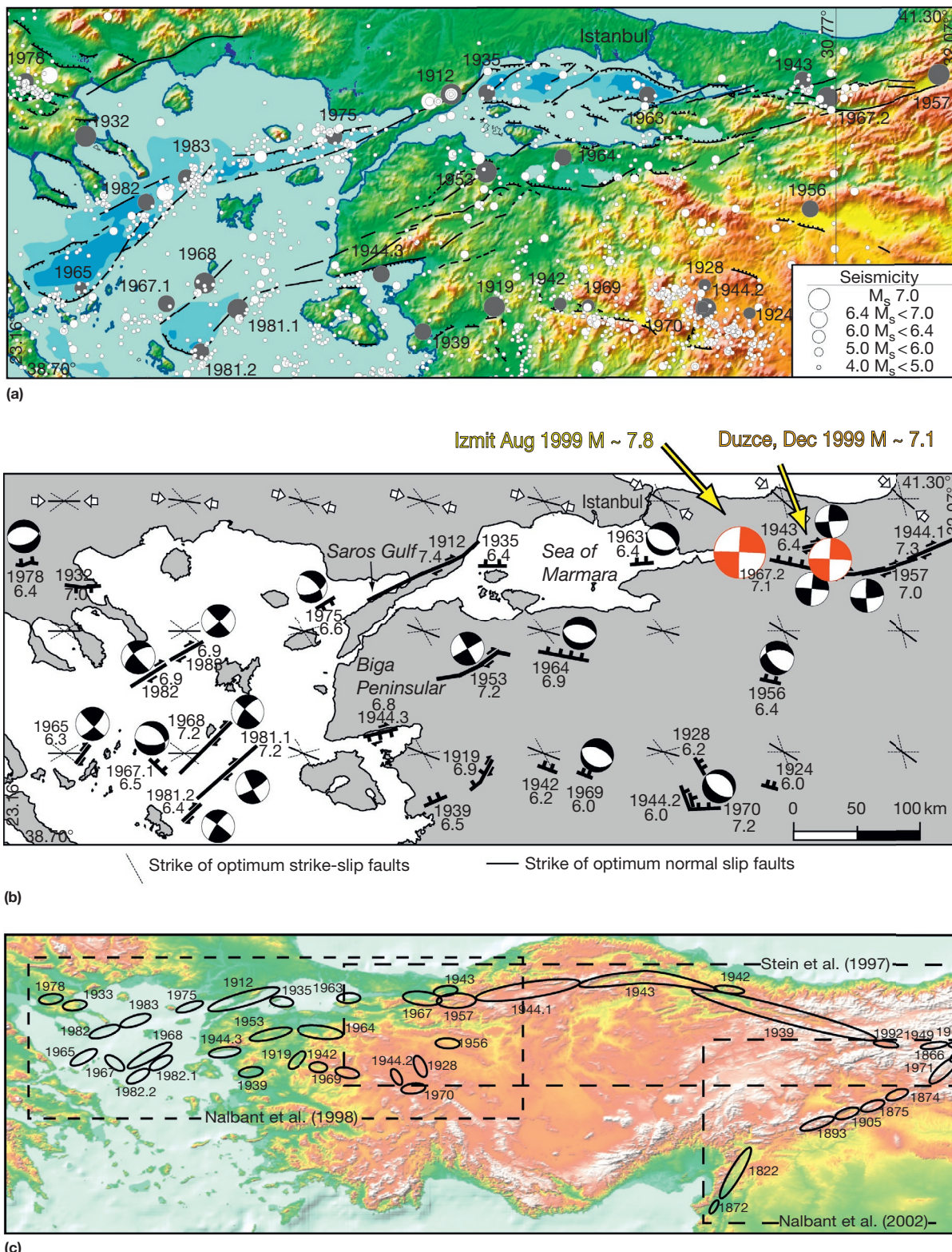


Figure 11 (a) Tectonic map of western Turkey and North Aegean Sea and distribution of seismicity between 1900 and 1996. (b) Fault plane solutions and active faults in the area (modified from Nalbant SS, Hubert A, and King GCP (1998) Stress coupling between earthquakes in northwest Turkey and the North Aegean Sea. *Journal of Geophysical Research* 103: 24469–24486). The orientation of the regional stress field used in the study is shown. Short solid lines indicate the orientation of the principal compressive stress. This is also the strike of optimally orientated normal faulting. The directions (two conjugate) for optimum strike-slip faulting are shown by lighter lines. (c) The regions and events studied by Nalbant et al. (1998), Stein et al. (1997), and Nalbant et al. (2002).

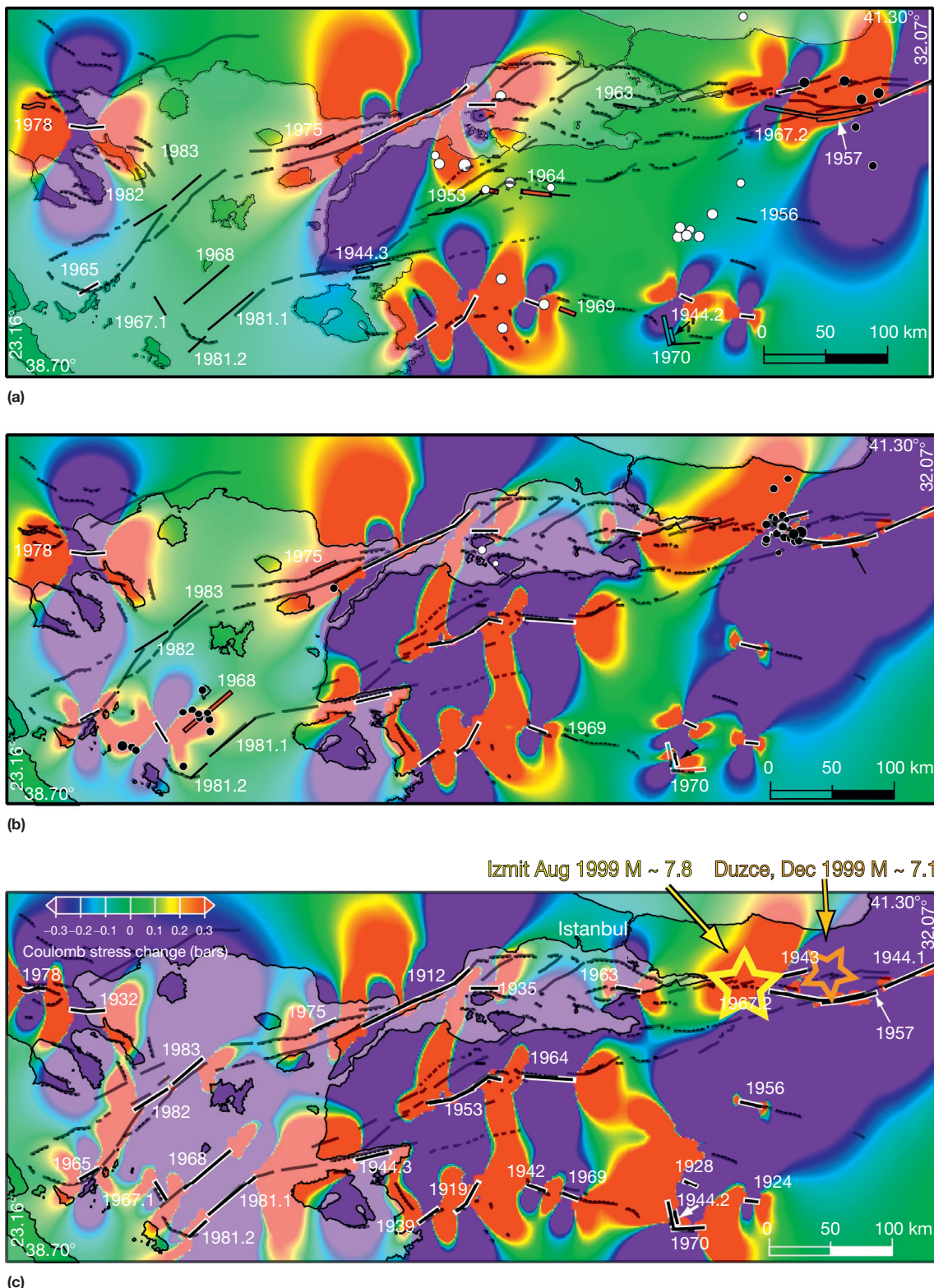


Figure 12 Coulomb stress changes on optimally oriented strike-slip and normal faults caused by earthquakes in subsequent time windows. The causative faults are shown in black lines enclosed with a white outline. Stress loaded faults are in red enclosed with a black outline. The faults in stress shadows are indicated in blue enclosed with a black outline. The black segments show those faults that are loaded by less than ±0.1 bar. Solid circles indicate aftershocks of some of the events, while open circles show background activity. (a) Stress changes caused by the events in the time window 1912–44 (1912, 1919, 1924, 1928, 1932, 1935, 1939, 1942, 1943, and 1944.1). (b) Stress changes caused by the events in the time window 1912–67 (the previous events plus those in 1944.2, 1944.3, 1953, 1956, 1957, 1963, 1964, 1965, 1967.1, and 1967.2). (c) Stress changes caused by the events in the time window 1912–96 (all the previous events plus those in 1968, 1969, 1970, 1975, 1978, 1981.1, 1981.2, 1982, and 1983). Four regions both showed increased Coulomb stress and included faults showing clear Holocene activity, part of the western Sea of Marmara, the western part of the Biga peninsula, the Saros Gulf, and the Izmit Bay region where the August 1999 (M_s 7.8) earthquake occurred.

are unlikely to experience an earthquake. Interaction studies of this sort are always limited by a lack of knowledge of events that preceded the time period studied. There are few cases in which a study can extend over a greater time period than the return periods of the earthquakes. This is the case of the study discussed in [Section 4.10.5.1](#).

The 1999 Izmit earthquake occurred in one of four regions (see figure caption) where known active faults and increased Coulomb stress coincided. When the Izmit earthquake struck, Coulomb stress on faults in the eastern Marmara Sea increased by between 1 and 5 bar as well as by about 1 bar to the east of the Izmit rupture zone ([Hubert-Ferrari et al., 2000](#)). On 12 November 1999, a second M 7.2 earthquake (Duzce) occurred in this eastern region (see [Figure 11](#)). It is important to note that this region was in a stress shadow prior to the Izmit earthquake that changed its status. Other examples of this sort are discussed by [Nalbant et al. \(1998\)](#). Thus, while stress shadows are in general less likely to host future earthquakes, their status can change if an event occurs in adjacent regions. The present situation in the Sea of Marmara region is discussed in [Section 4.08](#) where the effects of long-term loading are also included. A ~ 100 km stretch of fault south of Istanbul can now be identified as being likely to host a future earthquake.

The success of the Izmit and Duzce predictions together with the prediction of a M 8.7 event following the 26 December 2004 M 9.3 Great Sumatra Earthquake ([McCloskey et al., 2005](#)) provides three examples of Coulomb methods forecasting future events and forms an important part of the evidence establishing regions of enhanced Coulomb stress in places hosting known active faults as powerful approach to establishing medium-term seismic hazard for a region.

4.10.3.7 Interactions Between Very Large Earthquakes

Most of the earthquakes discussed earlier had lengths (L) that were not much greater than their down-dip width (W). Under these conditions, an earthquake on one segment of fault can

significantly modify the stress on all of a nearby segment. The distance to which the stress field extends, however, depends on the smallest fault dimension; thus, when the $L-W$ ratio becomes very large, the stress change affects only a small part of an adjacent fault segment at most ([Figure 13](#)) and thus the simple stress triggering described earlier is less likely to occur. Only if the epicenter where the next event initiates is close to the boundaries of slip of the previous earthquake is triggering unambiguous. For the North Anatolian fault sequence, six events had $L-W$ ratios > 10 and initiated close to the termination of a previous rupture. One event in 1943 initiated 230 km from the end of the rupture termination of the 1939 event and has not been regarded as being triggered by static stress changes ([Stein et al., 1997](#)). Because of the reduced role of stress interaction for large events, other effects, including loading ([Section 4.10.5.1](#)), seem to become more important for massive earthquakes.

4.10.3.8 Is It Better to Calculate Stress Transfer to Known Faults?

Most of the early studies of both aftershocks and stress interactions between large events used the formulation presented in [Section 4.10.2.3](#) to calculate optimum fault orientations based on a regional stress field. Where the fault planes of large events were known, this was commonly backed up by calculation of Coulomb stress change on the known fault (e.g., [Nalbant and McCloskey, 2011](#)). Some recent work has abandoned looking at changes on optimum planes considering it to be better to resolve the stress onto a target fault plane ([Steacy et al., 2005; Toda et al., 2008](#)). This is correct if an averaged fault surface represents the part of the fault where triggering occurs. Faults however are inherently complex, en echelon and multi-stranded on many scales and rupture may initiate on local complexities. Thus, it is unknown whether the stress change resolved on the fault plane as defined by its average surface trace or focal mechanism is more appropriate than the optimum direction. It should be recalled that stress directions are

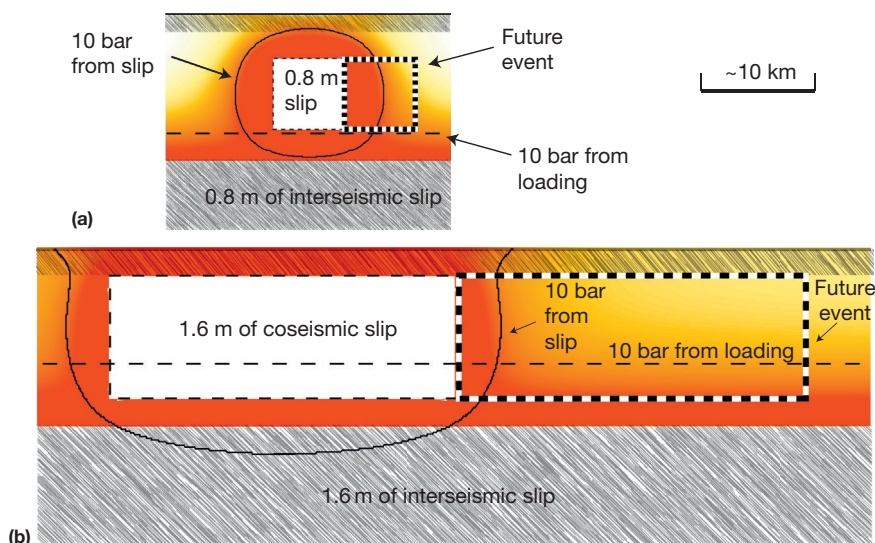


Figure 13 The relative contributions of long-term loading and seismic slip for events with length (L) to width (W) ratios of 1 and 4 for (a) and (b), respectively. The solid contour in each case indicates 10 bar of increase due to the earthquake and the dashed line 10 bar due to loading. Hatching indicates regions that slip aseismically. See also Figure 6 of Lin and Stein (2004).

derived from averages of fault directions and focal mechanisms for a region and hence may represent better those parts of a fault where slip can be triggered.

For small events and aftershocks, very large numbers of events can be examined if the optimum Coulomb condition is assumed providing a much larger data set. This could be seen as an advantage. However, since a certain knowledge of the stress system is never available, most authors have assumed that more than one mechanism is possible. An overall compressional or extensional regional stress field may allow some events to be strike-slip and not just prevailing dip-slip mechanisms. As a result, the maximum Coulomb stress for the two possible fields is chosen, for example, selecting the largest Coulomb stress increase for either strike-slip or reverse fault events. This enlarges the positive Coulomb lobes; thus, although some extra can be captured, better correlations may not be real.

Some of the errors associated with the study of aftershocks may be the failure to account for the stress changes resulting from the aftershocks themselves. Thus, the stress field from the main shock alone is inadequate to represent the stress field as an aftershock sequence evolves. The aftershock sequence can release a substantial fraction of the magnitude of the main event (Marsden and Nalbant, 2005). Clearly, the stress changes for the Big Bear aftershock could not be ignored when examining the seismicity following the Landers earthquake. However, most aftershocks are not localized in small clusters, and as the event sizes reduce, their area of influence diminishes rapidly. Consequently, except for some of the larger aftershocks, this should do no more than blur the boundaries of the main event Coulomb distribution. It certainly cannot account for events that clearly fall in regions where Coulomb stress is reduced by the main event.

As noted earlier for a number of cases, aftershock focal mechanisms are available, and a number of workers have carried out direct calculations and examined each of the two possible nodal planes and carried out various statistical tests. Perhaps surprisingly, the results have not proved to be much better than the earlier studies (see references in Steacy et al., 2005). In such tests, some aftershock sequences have worked quite well such as Landers, Superstition Hills, and Kobe, while others, notably Loma Prieta, have not. Later discussion may provide some of the reasons for the lack of improvement brought by approaches considering transfer on known faults rather than optimum directions and why studies of events such as Loma Prieta have not proved successful.

4.10.4 Introducing Time into the Failure Criterion

The results discussed so far assume that earthquakes can be represented by dislocation surfaces, that faults obey a Coulomb friction failure condition, that the lithosphere can be treated as a homogeneous, elastic half-space, and that the loading system consists of a simple stress field. The examples provided, plus many others in the literature, support the notion that stress changes due to motion on one fault can result in motion on a second. Despite examples demonstrating that other effects must also intervene, stress interaction must be an important element in any attempt to explain the most prominent feature of global earthquake statistics. Earthquake

pairs are clustered in space and time with the occurrence of one event increasing the probability of a second, with the probability decaying with distance and time from the first event (Kagan and Jackson, 1991). In the development so far, time has been absent and will now be considered in subsequent sections where more complex models are adopted. Since the failure criteria on faults are time-dependent, the lithosphere is inhomogeneous, and loading conditions are not simple stress fields, attempts to account for such effects introduce a wide range of possible models.

4.10.4.1 Time-Dependent Rock Failure

Failure in a rock sample does not occur at the peak stress, but occurs in a postpeak region when the system is mechanically weakening faster than the loading system can respond. Scholz (1990) explained that the mechanical breakdown associated with this weakening requires finite displacement before failure can occur. Because this breakdown or nucleation is quasistatic, it requires a finite time to occur. It is this *kinematic* feature of failure that introduces time into failure criteria. For rock samples, this is associated with the growth and interaction of defects with the largest defects being the most important (e.g., Ashby and Sammis, 1990). The effect is to be expected both for new failure in rock and for new failure on an existing fault surface. In the lithosphere, there is no way to establish a priori scale at which the breakdown process occurs; however, for large earthquake faults, this appears to involve large volumes of rock (Manighetti et al., 2004).

Since earthquakes are commonly regarded to result from new slip on existing surfaces, the behavior of such surfaces has been carefully studied in the laboratory, giving rise to 'rate- and state-dependent friction models.' These have been widely adopted and are effective in explaining many observations. While the mathematical formulation undoubtedly captures basic features of the underlying mechanical processes, it is important to remember that failure in the lithosphere could involve different process from a saw cut in granite.

4.10.4.2 Rate- and State-Dependent Friction Equations

Many formulations of rate- and state-dependent friction law have been proposed (e.g., Scholz, 1998 and references therein). In general, these constitutive laws can be described by two coupled equations. The first one relates the sliding resistance τ to the slip velocity V and the state variables θ_i ; it is usually named the governing equation,

$$\tau = F[V, \theta_i, A, B, \mu_0, \sigma_n]$$

where A and B are two positive parameters that depend on the material properties, temperature, and pressure. μ_0 is a reference friction value and σ_n is the normal stress. The second law provides the time evolution of the state variable and it is called the evolution equation. For a single-state variable, this becomes

$$\frac{\partial \theta}{\partial t} = G[V, L, \theta, B]$$

The state variable θ provides a memory for the sliding surface. A widely used formulation for these laws includes a single-state variable:

$$\tau = \mu_0 \sigma_n + A \ln \frac{V}{V^*} + B \ln \frac{\theta}{\theta^*}$$

$$\frac{\partial \theta}{\partial t} = 1 - \frac{\theta}{L} V$$

These equations have been proposed to model earthquake after effects and they have been used to predict aftershock rates (e.g., Dieterich, 1994), to study stress shadowing (e.g., Harris and Simpson, 1996) as well as stress triggering (e.g., Gomberg, et al., 1998). Subevent triggering can occur over several hours, days, or weeks, as observed, for instance, during the 1992 Landers earthquake. During such short triggering times, the remote tectonic load is not playing any role. For longer periods, loading must be considered. The relation between short-term effects of rate and state friction and longer-term loading is illustrated in Figure 14 modified from Stein et al. (1997). In Figure 14(a), the Coulomb stress ahead of the fault is shown to increase steadily as a result of tectonic loading at a point x until it increases abruptly because of an earthquake on an adjacent fault after which it returns to the same rate. In a simple model of repeating earthquakes, a new event occurs when a threshold is crossed. The threshold is shown to be blurred to indicate that in practice, the recurrence time is irregular and has to be expressed in statistical terms – a mean and standard deviation, for example. Thus, at any given time, the probability of an earthquake in any time period depends on where the stress on the fault lies in the earthquake cycle. Shortly after an earthquake, the probability of an event is low, and as the mean recurrence time is approached, the probability

of a second event being triggered increases. The simple result of the stress step is to apparently advance the proximity to the mean recurrence time and thus increase the probability that an event will occur.

The transient effects predicted by rate and state friction behave differently (Figure 14(b)). It is assumed that nucleation processes on and around the fault are promoted by the coseismic stress step. It thus increases the chance to trigger the fault rupture immediately after the earthquake but rapidly decays following Omori's aftershock curve. This then results in a much-greater increase of probability than the simple recurrence time model (Stein, 1999).

Numerous studies have adopted this approach. However, a study that uses the rate and state model to predict both the rates of small earthquakes and the probabilities of larger events has been published by Toda et al., 2005 accompanied by an animation that follows the evolution of seismicity in Southern California between 1986 and 2003. The study provides an articulate description of the use of rate and state friction (<http://sicarius.wr.usgs.gov/landers>).

4.10.5 Loading Models and Lithospheric Properties

4.10.5.1 Elastic Half-Space Loading and Stress Relaxation Models

In the introduction, two categories of lithospheric models were described: one with faults or localized shear zones extending to

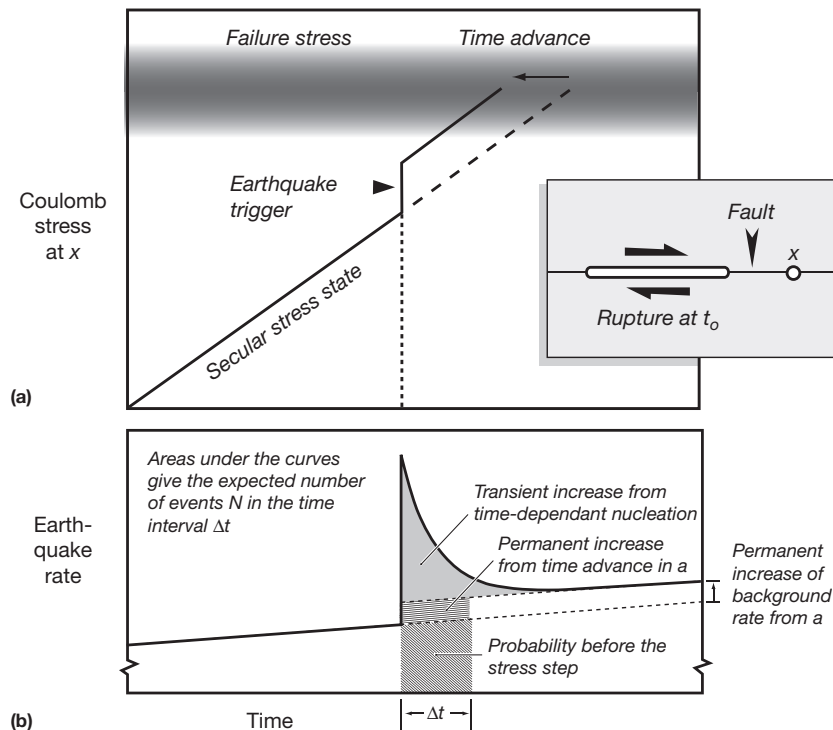


Figure 14 Schematic illustration of a sudden stress increase on a fault at point x near to an earthquake rupture at time t_0 (inset). (a) The stress increase advances the time to the next rupture. If the stress was closer to failure at the time of the stress step, then the stress step could have triggered the event immediately. (b) The associated short-term (transient) and long-term (permanent) increase in the rate of earthquake occurrence. This can also be interpreted as an increase of probability of a large event. Modified from Stein R, Barka AA, and Dieterich JH (1997) Progressive failure on the North Anatolian fault since 1939 by earthquake stress triggering. *Geophysical Journal International* 128: 594–604.

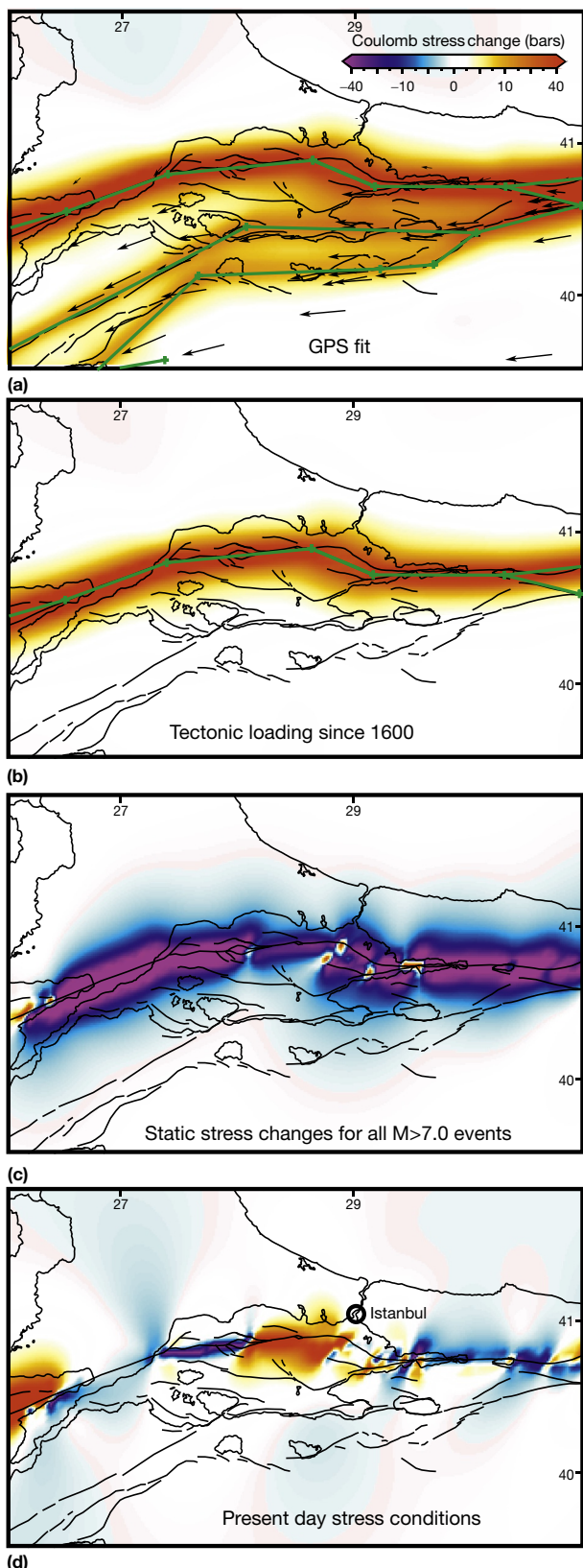


Figure 15 Accumulated loading and stress loading for the Marmara Sea region from 1600 to 2000. (a) Loading rate based by fitting GPS vectors for all branches of the Anatolian Fault around the Sea of Marmara. The panel only shows a part of region studied to determine the

the asthenosphere and the second with viscous deformation occurring in the lower crust and below. Both of the approaches with various adaptations have been introduced to explain the long-term effects of loading and shorter-term time-dependent effects following big earthquakes.

From the point of view of Coulomb calculations, the widely adopted models assume that a fault continues below seismogenic depths and between earthquakes moves at a constant rate. Where a sufficient span of GPS data is available, the model used to explain geodetic observations can be used directly to generate long-term loading. An example is shown in [Figure 15\(a\)–15\(d\)](#) adapted from [Pondard et al. \(2007\)](#) that considers loading and earthquakes since 1600 for the Sea of Marmara region. [Figure 15\(a\)](#) and [15\(b\)](#) shows the stress loading based on the rate defined by GPS measurements that are also consistent with longer-term geologic rates. [Figure 15\(c\)](#) shows the stresses due to the earthquakes alone and [Figure 15\(d\)](#) combines these with the loading ([Figure 15\(b\)](#)). An ~100 km stretch of fault in the Sea of Marmara is now stressed and represents an earthquake hazard to Istanbul. Stress change and loading models of this kind have also been adopted to provide the parameters needed to estimate the probabilistic seismic hazard discussed in [Section 4.08](#) ([Parsons, 2004](#)).

The creeping fault at depth is assumed to have a velocity hardening behavior and can consequently be expected to slip at a greater rate following an earthquake (e.g., [Perfettini and Avouac, 2004](#)). This after-slip should introduce steadily increasing stresses following an earthquake and particularly for events with large $L-W$ ratios should cause the stressed region to expand with time (e.g., [Stein et al., 1992](#)). The effect of this evolving stress field offers a way to explain the time evolution of aftershocks that differs from that suggested by rate and state friction ([Section 4.10.4.2](#)). However, viscous relaxation at depth and fluid flow processes are also candidates as discussed later and in [Sections 4.10.5.2](#) and [4.10.5.4](#).

Stress relaxation in viscous lower crust has been proposed to explain at least some aspects of the time-dependent effects associated with aftershocks and delayed triggering of more distant large events (e.g., [Chery et al., 2001](#); [Freed and Lin, 2001](#); [Nalbant and McCloskey, 2011](#); [Parsons et al., 2008](#); [Pollitz et al., 2004](#); [Toda et al., 2008](#)). The effect, however, is difficult to distinguish in terms of the evolving stress field to the assumption that increased post-earthquake slip occurs on a fault at depth. The approach has proved successful to explain earthquake interactions in Mongolia and the 2008 Wenchuan, China, earthquake. In particular, this approach has been adopted to explain clusters of large earthquakes on the assumption that stress progressively spreads slowly from the epicentral region. The apparent success does not demonstrate that the approach is necessarily correct. [Peltzer et al. \(1998\)](#) pointed

rates ([Flerit et al., 2003](#)). The inset scale bar corresponds to a time period of 400 years and is the same for all subsequent panels. The GPS vectors are shown as arrows and green lines identify the slipping faults beneath the locking depth. (b) The loading for the northern branch alone for 400 years. (c) Stress changes resulting from all earthquakes $> M 7.0$ since 1600. Smaller events are of little significance. (d) The combined effect (summed) of loading and stress changes due to events. The stressed region south and west of Istanbul is expected to host a future $\sim M 7$ earthquake.

out that the evolution of the vertical component of the displacement field determined from satellite-based radar is not consistent with these models. Furthermore, the behavior of the lithosphere is generally contentious (e.g., Jackson et al., 2008).

How stress is transmitted to the platelike brittle crust through the thick low viscosity lower crust proposed by authors such as Royden et al. (2008) is not easily understood nor how significant faults can develop in these models. Studies of stress interactions in loaded 2D loaded plates discussed in the next section might suggest how fault localization can occur.

4.10.5.2 2D Platelike Models

Typically, models consider the plate to be driven at a distance by displacement boundary conditions and viscous effects are ignored. Faults or deformation zones evolve in the plate as a result of purely elastic interactions between a distribution of initial defects that grow and interact by obeying a simple failure law. Studies of this sort adopt automata modeling (e.g., Ferguson et al., 1999; Olami et al., 1992; Rundle et al., 1995). These approaches assume that the seismogenic layer is 100% seismogenic and all earthquakes are a consequence of earlier events. This assumption also underlies models that call on ‘self-organized criticality’ and is an underlying justification for concepts such ‘epidemic-type aftershock sequence’ models (e.g., Helmstetter and Sornette, 2002; Ogata, 1988, 1989; Ogata et al., 2003). These models are proposed to have a universal application (e.g., Helmstetter and Sornette, 2002; Helmstetter, et al., 2003; Ogata, 2004; Sornette and Helmstetter, 2002).

While these techniques may produce a useful statistical approach to characterizing earthquake catalogs and some insight into interaction processes, a problem lies in differences in interaction between faults with small and large $L-W$ ratios and their coupling to loading processes resulting from stable sliding both within and beneath the seismogenic zone. This is summarized in Figure 16. Figure 16(a) shows that the stick-slip region does not come fully to the surface and even within the seismogenic region patches of stable sliding can occur. This effect can be seen in the depth distribution of slip contributed by events at different depths (Figure 16(b)). Near to the surface and near the base of the seismogenic layer stick-slip events contribute only a modest amount of slip (King et al., 1994a). In creeping regions such as central California, only a few percent of the slip is seismic and occurs on a few patches (Figure 16(c)). Events in such regions are too widely separated to interact (Figure 16(d)). Unlike the situation shown in Figure 13 in the center of a noncreeping seismogenic zone where interactions are strong, it seems that complete stress coupling and stick-slip behavior can only occur in a narrow region in the center of a seismogenic zone. Since events of $M \sim 6$ completely cut the seismogenic zone, only much smaller events in a narrow depth range can be considered to be dominated by elastic interactions alone. The related problem of large earthquakes not belonging to the same fractal set as small ones is considered by Scholz (1990) and Pacheco et al. (1992).

4.10.5.3 Inhomogeneous Lithospheric Models: The Effects of Voids or Fissures

The most dramatic inhomogeneity that can be introduced in a solid is a void, which can contain volcanic magma, water, or

gas. A familiar feature of volcanic or thermal regions is the earthquakes that occur very close to a volcanic vent or hot springs. The b -value of the Gutenberg–Richter relation associated with such earthquakes is commonly high – a large number of small events occur for each larger event. Expressed in terms of moment release, small events account for as much deformation as large events unlike the seismicity of nonvolcanic regions (see also Section 4.10.5.5). The same character is shared by the seismicity of creeping faults, and in both cases, the deformation associated with the seismicity is tiny compared with that due to nonseismic processes (see also Figure 16). The most straightforward explanation is that earthquakes in volcanic regions like those on creeping faults are not interacting, being separated by voids that deform aseismically. Sibson (2002) offered a hypothetical geometry for such processes based on the work of Hill (1977).

4.10.5.4 Interactions Between Volcanic Eruptions and Earthquakes

Since volcanic fissures or magma chambers can be treated using dislocation theory, the techniques described for the interaction between large earthquakes can be modified to examine interactions between volcanoes and earthquakes and vice versa. Unlike earthquake faults, however, the plumbing of volcanoes is less well understood. It is not clear whether an eruption should be regarded as resulting from an increase of magma pressure forcing magma to the surface or a reduction of normal stress allowing fissures to open and the magma to reach the surface. It is similarly not clear whether the magma is contained in quasi-spherical chamber or in fissures. The various possibilities result in different stress fields whether examining the triggering of eruptions by earthquakes or the reverse. Notwithstanding these possible ambiguities, plausible relations between static stress changes associated with earthquakes and eruptions have been proposed for Djibouti and Italy (e.g., Noir et al., 1997; Nostro, et al., 1998; Walter and Amelung, 2007). Relations between volcanoes and earthquakes including dynamic and viscoelastic effects are reviewed by Hill et al. (2002).

4.10.5.5 Fluid Movement in Nonvolcanic Regions

Substantial evidence is accumulating for the mobilization of water in the seismogenic crust following major earthquakes both close to the active fault and in a region extending for several fault lengths from the epicenter. Direct evidence is derived from water expelled at the surface by the compressional elastic rebound of normal faulting earthquakes (Muir-Wood and King, 1993). Monitored changes of river flows finds that the increased flow progressively decays over 6–10 months (Figure 17). Comparing the volume of water expelled to the volumetric strain calculated from a source known from seismic and geodetic data indicates that a substantial proportion of the coseismic stress is relaxed by fluid flow. The volume expelled and the time constants involved suggest that the water is held in a connected system of high-aspect-ratio cracks. The importance of fluid flow is also suggested from geodetic studies of post-earthquake relaxation (e.g., Jonsson et al., 2003; Peltzer et al., 1998). As noted earlier in these cases, the relative effects of relaxation in a viscous lower crust, post-earthquake creep on

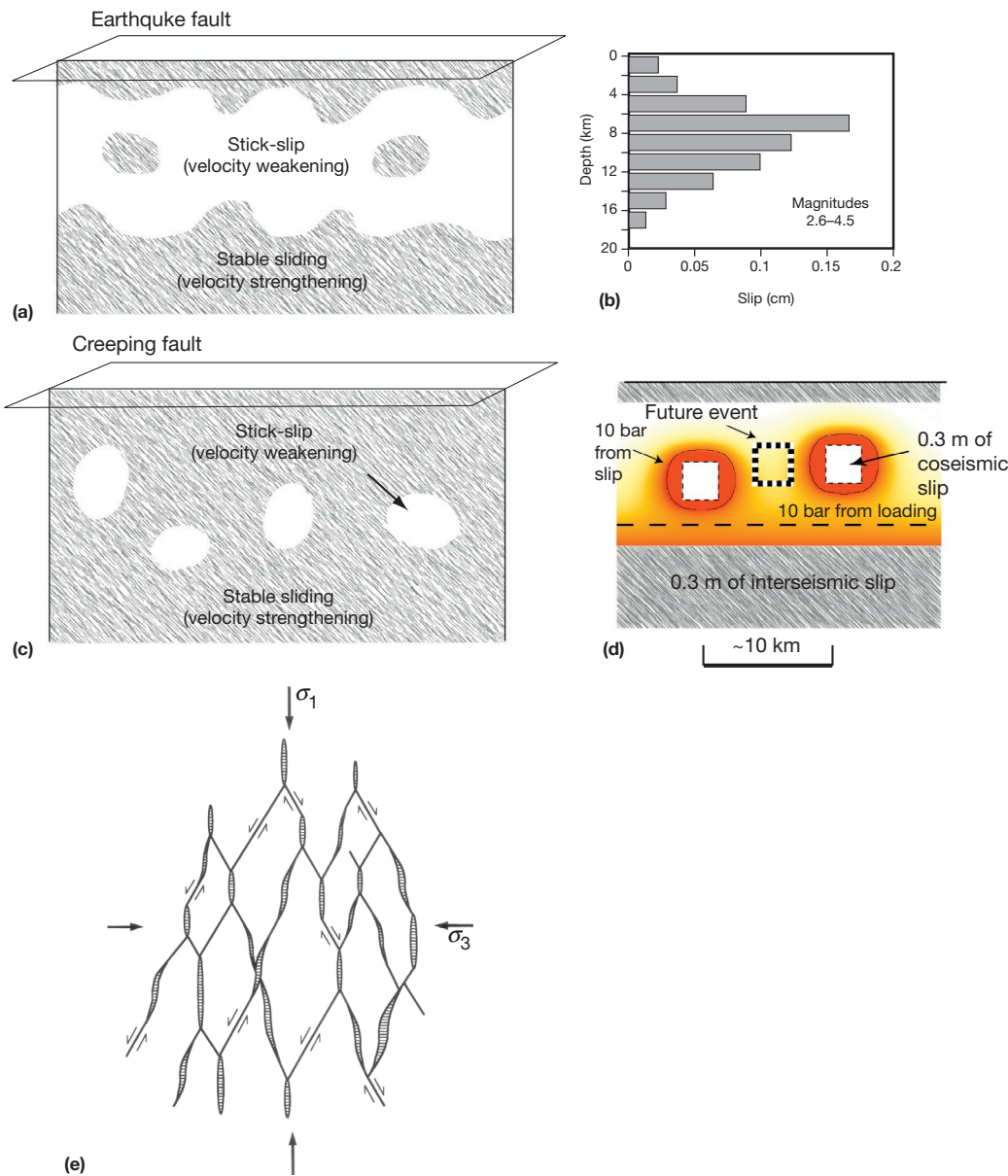


Figure 16 (a) Strike-parallel longitudinal section showing schematically regions of stick-slip and stable sliding. (b) The depth distribution of slip for events with magnitudes between 2.6 and 4.5 for the San Francisco Bay Area. The seismic slip is concentrated around 8 km. Similar results are found for other magnitude ranges (King et al., 1994a), indicating that at shallow and greater depths in the seismogenic zone, much of the deformation is aseismic as indicated in (a). A discussion of the depth of seismicity within the seismogenic zone can be found in Pacheco et al. (1992). (c) Strike-parallel longitudinal section showing schematically regions of stick-slip and stable sliding for a fault where aseismic creep predominates. (d) For a creeping fault, small stick-slip regions are too far apart to interact by stress coupling. (e) A mesh model for swarm seismicity involving interlinked minor faults and extension fractures infilled with dikes, hydrothermal veins, etc. (crosshatched), developed in relation to the principal compressive stresses, $\sigma_1 > \sigma_2 > \sigma_3$. Reproduced from Hill DP (1977) A model for earthquake swarms. *Journal of Geophysical Research* 82: 1347–1352.

a lower crustal fault and the effects of water flow are not easily separated.

The importance of the fluid flow suggested by these studies indicates that it must play some controlling role in aftershock sequences, and the time period of about 8 months is similar to the length of aftershock sequences. Two effects may control seismicity. The first is a change of the effective friction due to changes of fluid pressure (eqn [6]; e.g., Nur and Booker, 1972), thus altering the rate and distribution of seismicity predicted from Coulomb stress changes alone. While the Coulomb stress

distribution may not be greatly changed, fluid pressure changes may be an important alternative to rate and state friction to explain temporal changes. Furthermore, increases of pressure could trigger events in regions where reduced Coulomb stress predicts an absence of activity.

The suggestion that water is contained in high-aspect-ratio cracks and changes in pressure over a period of several months indicate that the effective rock modulus will change over a similar period. Since water is held in cracks whose orientation reflects the prevailing stress field, the modulus changes can be

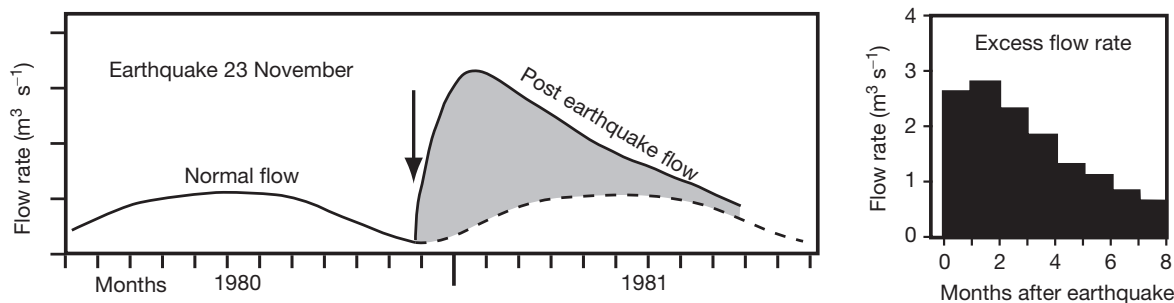


Figure 17 Excess flow for the Caposele spring resulting from compressional elastic rebound following $M_s 6.9$ Irpinia earthquake 1980. The form of the excess flow is typical for normal faulting events. Reproduced from Muir-Wood R and King GCP (1993) Hydrological signatures of earthquake strain. *Journal of Geophysical Research* 98: 22035–22068.

expected to be anisotropic. Such readjustments may be expected to generate stress fields and hence seismicity that are not simply related to a regional stress field or the Coulomb Stress change field following an earthquake. Several publications on the topic can be found in the review papers in the introduction. Of particular interest are recent observations of a correlation between the monsoon and midcrustal seismicity in the Himalayas (Bollinger et al., 2007) and an aftershock sequence driven by high-pressure carbon dioxide rising from depth (Miller et al., 2004).

4.10.5.6 The Distribution of Small Events Before Large Earthquakes

The aftershocks that result from a large earthquake are unambiguously due to stress increases that result from the event (Section 4.10.3). Over longer periods of time, there is also clear evidence for earlier large earthquakes setting up the stress conditions that control future large events. In the case of the Landers earthquake, smaller events also appear to have loaded the site of the future event (Figure 8 and associated text). The effect of long-term loading is also important and becomes progressively more significant for events with a large L - W ratio where interactions become less important (Section 4.10.3.7). Since the 1980s, considerable interest has been directed to the study of accelerated moment release (AMR) (e.g., Jaumé and Sykes, 1996), where activity is found to increase over a region with dimensions several times greater than the fault length (L). A range of explanations have been offered to explain the observations. Two relate directly to the concept of stress interactions. In the first, stress triggering between small events is considered to progressively create a stress field sufficiently homogeneous over a large enough region to host a big earthquake. The process is considered to be a manifestation of self-organized critical behavior. This attractive model is unfortunately difficult to relate to the observations of the geologists, geodesists, or seismologists who observe large earthquakes repeating on readily identified faults. Some of these problems have been addressed by the conditional criticality model (Bowman and Sammis, 2004).

A second explanation attributes the increase of activity as the consequence of the stress in a wide region increasing toward failure to be the consequence of the final stages of reloading a fault. This can be thought of as the final refilling of an earthquake shadow resulting from an earlier event. The

final process of loading is shown schematically in Figure 18 (King and Bowman, 2002; Scholz, 1990), with activity progressively increasing as the stress shadow fills.

Following an earthquake, the region that must have been loaded prior to the event can be calculated in a similar way to that used to identify post-earthquake Coulomb stress increases but by slipping the fault in the opposite direction to the slip that occurred in the event. It should be appreciated that this back-slip approach (Savage, 1983) models only the large-scale stress field that drives the earthquake. More local stress fields associated with fault complexity that progressively produce topography are not modeled in this way (e.g., Perfettini and Avouac, 2004). For all the events with magnitude >6.5 in California, an acceleration of activity has been found. When compared to random catalogs, the individual probability that the AMR for each event is a physical effect is modest. However, the cumulative probability that all events show AMR as a result of random processes is $<1\%$. Hardebeck et al. (2008) argued that it has no significance compared to their synthetic catalogs. The AMR in the far-field region of the 26 December 2004 Sumatra earthquake prior to the event (Figure 19) had $<2\%$ probability of being random (Mignan et al., 2006). While for Californian events with L - W ratios of ~ 3.5 , effects other than loading can possibly be invoked to explain AMR, for the Sumatra event with an L - W ratio of ~ 35 , loading seems the only plausible explanation for the observed pre-event increase of seismic activity.

4.10.5.7 Stress Inhomogeneity Resulting from Displacement Boundary Conditions

The foregoing sections have assumed that it is possible to define a regional stress field and steadily increasing stress due to tectonic loading. This is only perturbed by motion on known faults and it is these stress changes that trigger earthquakes. Calculations performed using the mathematics of dislocations in a homogeneous elastic half-space are assumed to provide an adequate approximation.

Prior to the success and popularity of Coulomb stress triggering models, other kinematic explanations for off-fault aftershocks had been suggested. These were based on a realization that distributed seismicity can be due to the fragmentation that results from a homogeneous material being subject to certain displacement boundary conditions (see King, 1986; King and Nabelek, 1985). While this approach has been eclipsed by the

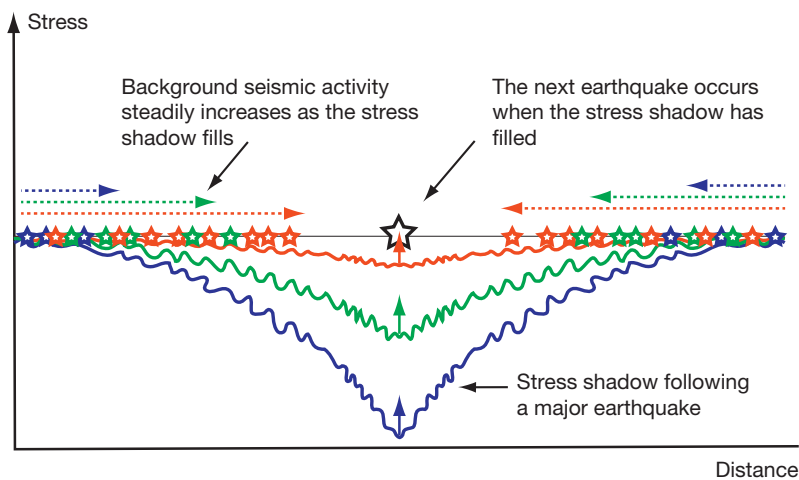


Figure 18 Following a large earthquake, a stress hole or shadow is created around the associated fault (blue line). This progressively fills (green then red lines) until the next major earthquake occurs. For the filling of the stress shadow for events with large $L-W$ ratios, the effect of aseismic creep at depth predominates. As the stress shadow fills, activity increases over a wide region. Modified from Scholz C (1990) *The Mechanics of Earthquakes and Faulting*. New York: Cambridge University Press, 439 pp; King GCP and Bowman DD (2002) The evolution of regional seismicity between large earthquakes. *Journal of Geophysical Research* 107: 2354.

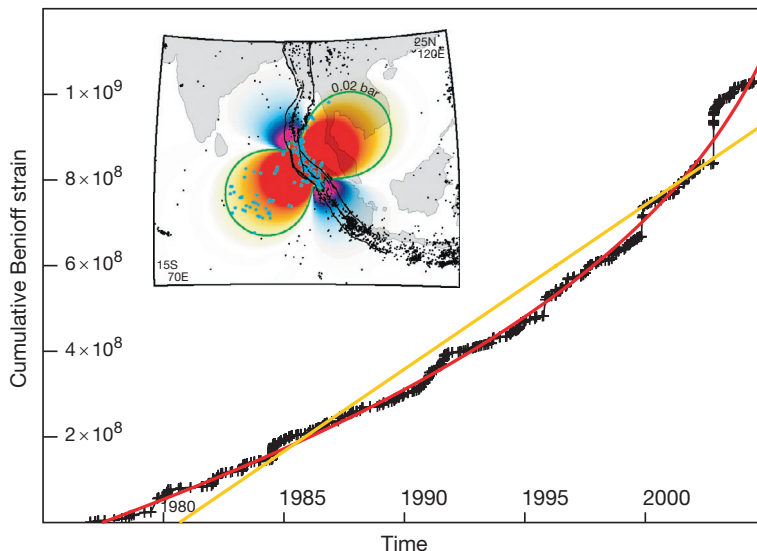


Figure 19 Accelerating moment release (AMR) for the great Sumatra earthquake of 26 December 2004. The cumulative Benioff strain and the time (in years) are, respectively, the y -axis and x -axis. The power law fit (red curve) has less than a 2% probability of occurring randomly. The prestress field calculated by the back-slip earthquake method for the high-slip part of the 26 December 2004 event is shown in the inset. The red contour (0.02 bar) outlines the area of events that provides the AMR. The fault used has four pure dip-slip segments each with a dip of 11° , a down-dip width of 200 km. Reproduced from Mignan A, King GCP, Bowman D, Lacassin R, and Dmowska R (2006) Seismic activity in the Sumatra-Java region prior to the December 26, 2004 ($M_w=9.0-9.3$) and March 28, 2005 ($M_w=8.7$) earthquakes. *Earth and Planetary Science Letters* 217: 339–408.

stress transfer models described in earlier chapters, it remains important for developing a fuller appreciation of how faults interact. The underlying concepts are summarized in Figure 20. Figure 20(a) shows that for simple shear displacement boundary conditions, motion can be accommodated by strike-slip faults with a single strike direction. For simple contraction or extension (Figure 20(b)), antithetic dip-slip faults can also, in principle, accommodate long-term motion provided the faults completely cut from the surface to a depth at which stress is relaxed by flow. In these two cases, the faults are kinematically stable because they release the boundary conditions by

accumulating finite displacement without changing geometry. But no other boundary conditions can be accommodated in such a simple way (Figure 20(c)). A system of faults with various orientations must come into existence even though the material was previously homogeneous and unfractured. Where these faults meet kinematic incompatibility requires further multiple faulting.

The behavior of this faulting can be examined using a generic model of three strike-slip boundaries meeting at a triple junction, a system identified to be always unstable (McKenzie and Morgan, 1969). In a plate tectonic context, one or more of

the boundaries must allow the creation or destruction of plate area (i.e., must be ridges or trenches) for a triple junction to be stable and evolve in a straightforward way. In general, deforming continental lithosphere lacks such sources and sinks so the evolution of a three-fault triple junction evolution is complex (illustrated in [Figure 21](#)). In [Figure 21\(a\)](#)), finite fault slip

requires a volume change at the junction. In the lithosphere, however, high confining pressure prevents large volume changes and deformation must accumulate off the main faults ([Figure 21\(b\)](#)). Although small deformation can be accommodated elastically, substantial deformation must be accommodated by fracture ([Figure 21\(c\)](#) and [21\(d\)](#)). The predicted

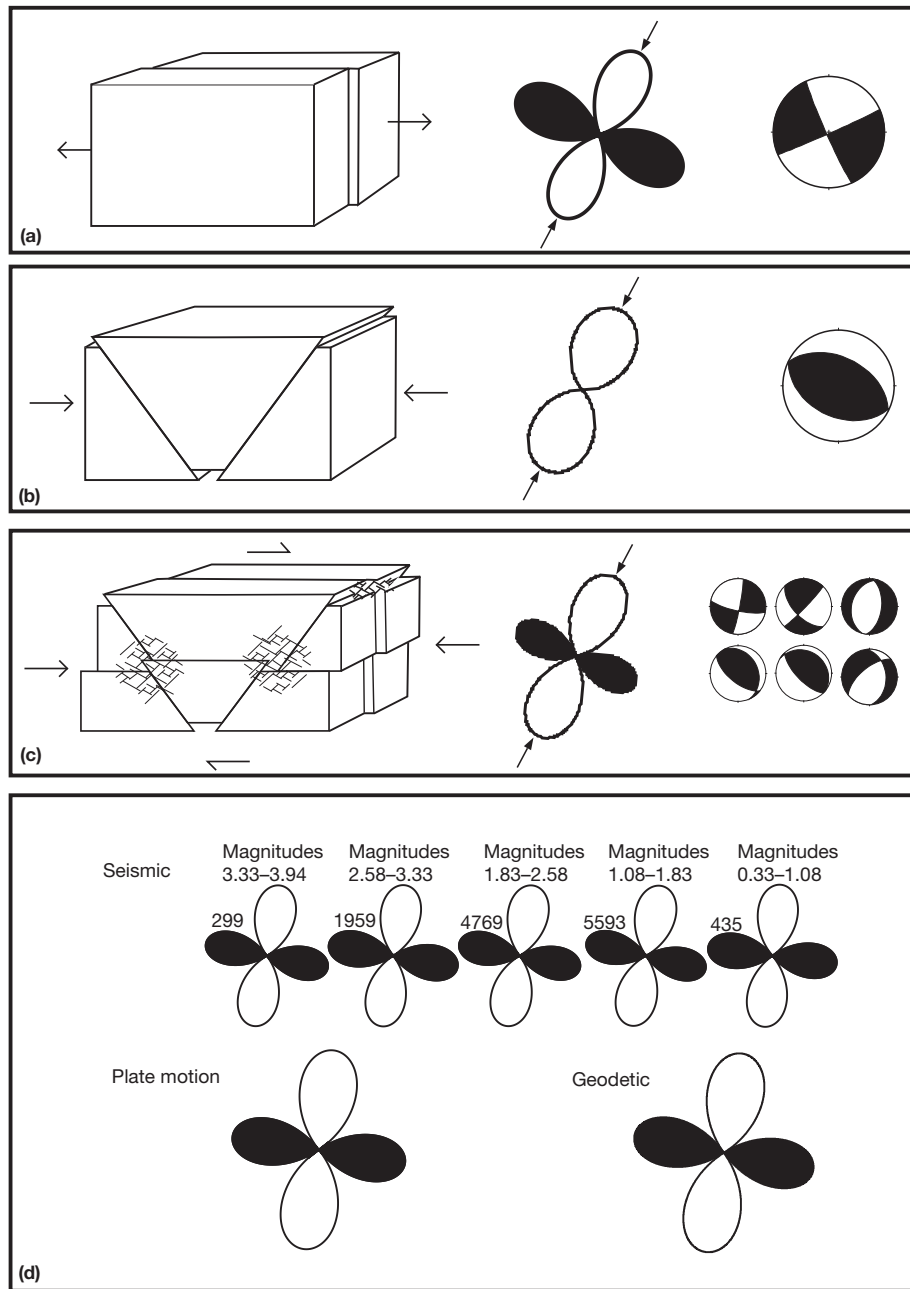


Figure 20 The kinematics of finite strain. (a) Simple shear displacement boundary can be released on a single fault. The associated strain rosette and focal mechanism are shown. (b) Simple contraction can be relieved (under certain circumstances) by simple dip-slip faulting. The associated strain rosette and focal mechanism are shown. (c) More complex displacement boundary conditions require multidirection faulting indicated schematically. The strain rosette can only result from numerous earthquakes with different mechanisms operating together. The mechanisms shown are typical of the heterogeneous aftershocks for the Loma Prieta earthquake. (d) The seismic strain can be represented by examining earthquakes in magnitude windows each of which includes earthquakes that change average fault length by a factor of 2. The distribution of finite strain released by small events has the same form as that predicted from plate motion and determined geodetically. Parts of the figure are adapted from Amelung F and King GCP (1997) Large scale tectonic deformation inferred from small earthquakes. *Nature* 386: 702–705.

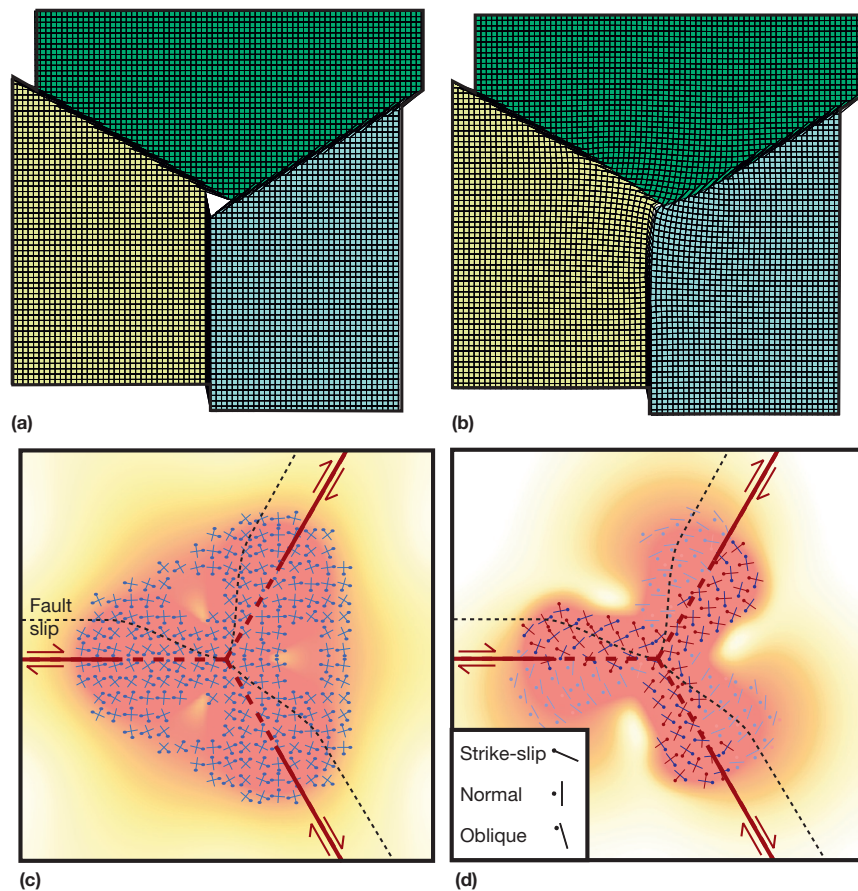


Figure 21 Junctions between strike-slip faults are kinematically unstable (McKenzie and Morgan, 1969). They are however observed at the Earth's surface (e.g., junctions between the North and East Anatolian Faults in Turkey). The deformation associated with such junctions can be accommodated in two ways. (a) A void is created. The faults separate three undeforming blocks. (b) In the Earth's lithosphere, however, confining pressure prevents large volume changes. At the junction, slip must come to zero forcing deformation to be accommodated off the main faults. (c) For a plane strain model (2D), the shear strain (in red) induced around the junction by motion on the main faults is shown. Dashed curves illustrate the slip distribution on the main faults. Slip comes to zero at the junction between the three faults. Symbols represent the predicted slip directions (see Figure 7; Devès et al., 2011 and inset below in Figure 24). Whereas mechanisms are all strike-slip, they present different directions preventing localization to occur on long distances. Deformation can only be accommodated in a distributed manner, which can occur, for instance, by motion on many small faults (or shear zones) with different directions. (d) For a plane-stress model with a compressional out of plane principle strain, the strain distribution is changed and some mechanisms are normal faulting, but again deformation has to remain distributed; localization cannot develop on long distances. Figure reproduced from Devès M, King GCP, Klinger Y, and Amotz A (2011) Localised and distributed deformation in the lithosphere: Modelling the Dead Sea region in 3 dimensions. *Earth and Planetary Science Letters* 308: 172.

directions of fracture are shown in these figures and can be seen to change from place to place around the junction. No fault can grow to a substantial length; therefore, deformation is taken up by small-scale faulting occurring in multiple directions. In two dimensions, three directions must exist to accommodate the strain, and in three dimensions, five directions must exist (King, 1983). Small-scale faults also interact to create areas of kinematic instability resulting in multiple faulting at ever-smaller scale. At the scale of the main strike-slip faults, however, off-fault deformation appears to be uniformly distributed around the junction. The term 'process zone' has been used to refer to these areas (e.g., Devès et al., 2011; Scholz, 2002).

While the triple junction of Figure 21 provides a simple example, other geometric complexities such as fault bends,

offsets, or intersections are all places of kinematic instability requiring some deformation to occur in a distributed manner (King and Nabelek, 1985). Figure 20(a)–20(c) shows that three deformation systems can have the same principle axis of shortening, but in the case of Figure 21(c), several different focal mechanisms must operate to generate the observed azimuthal strain distribution (strain rosette). The earlier assumption that the principle stress axes uniquely define the orientation of fault planes is not correct and the multifault deformation described requires that the concept of a temporally constant regional stress field should be abandoned. Stresses must be both inhomogeneous in space and evolve with time. The observation of complex fault mechanisms is a consequence of the kinematics of finite deformation and not as

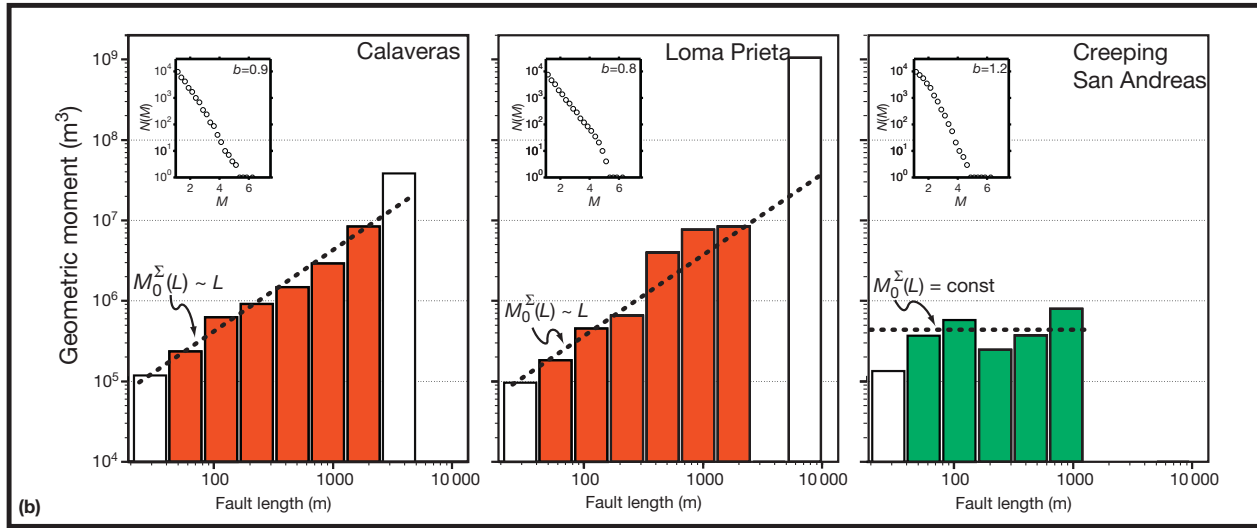
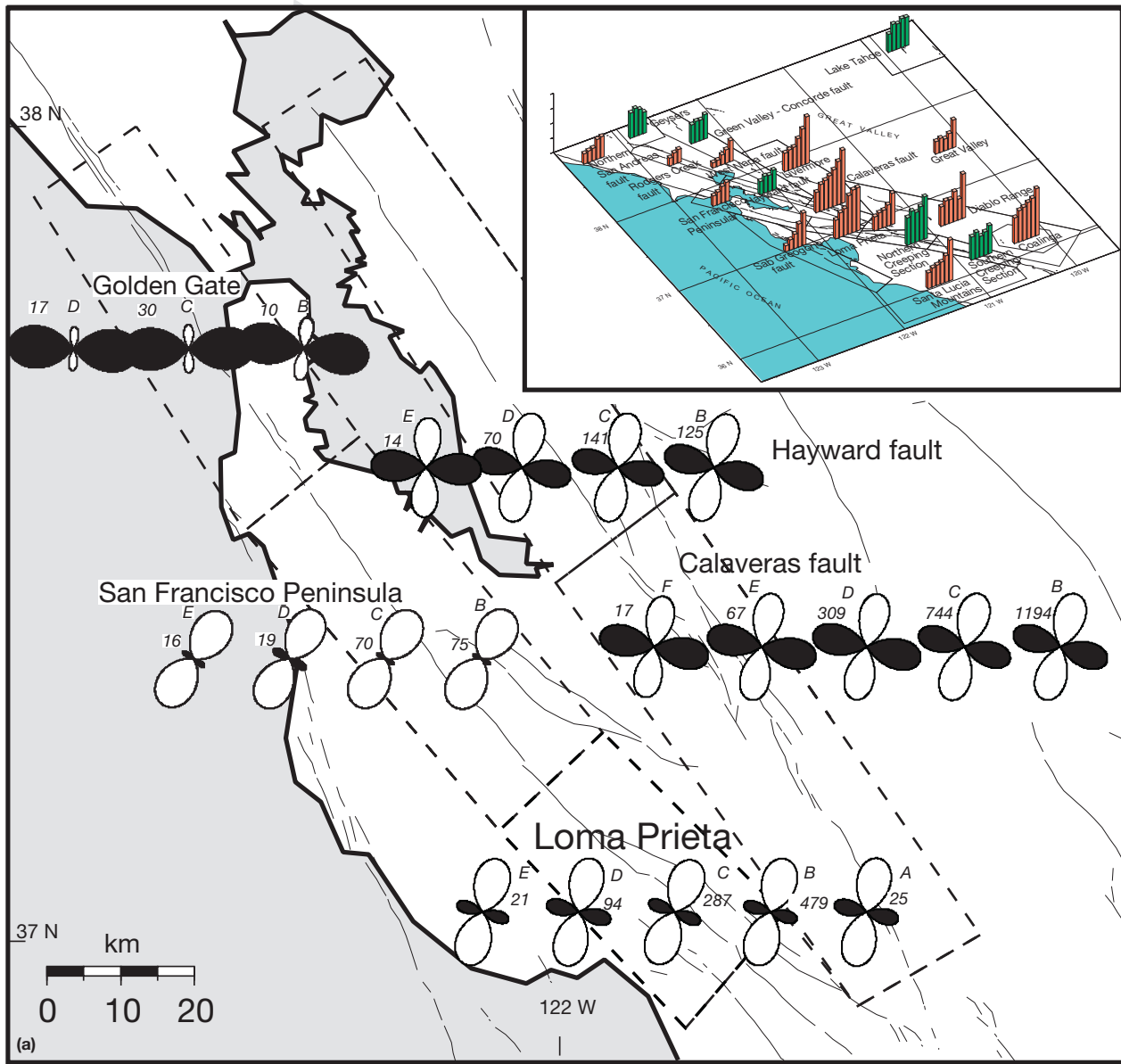


Figure 22 Earthquake kinematics for the San Francisco Bay Area. The strain rosettes are created by separating events into bins with average fault dimensions differing by factors of 2 (as described in the caption to Figure 17). Although the overall finite strain summed for the whole region is the same as the applied boundary conditions (Figure 17(d)), there are substantial local variations. (b) The scaling relations for the summed geometric moment (potency) in the bins described earlier, for example, regions. For noncreeping regions, the moment release doubles for each factor of

(continued)

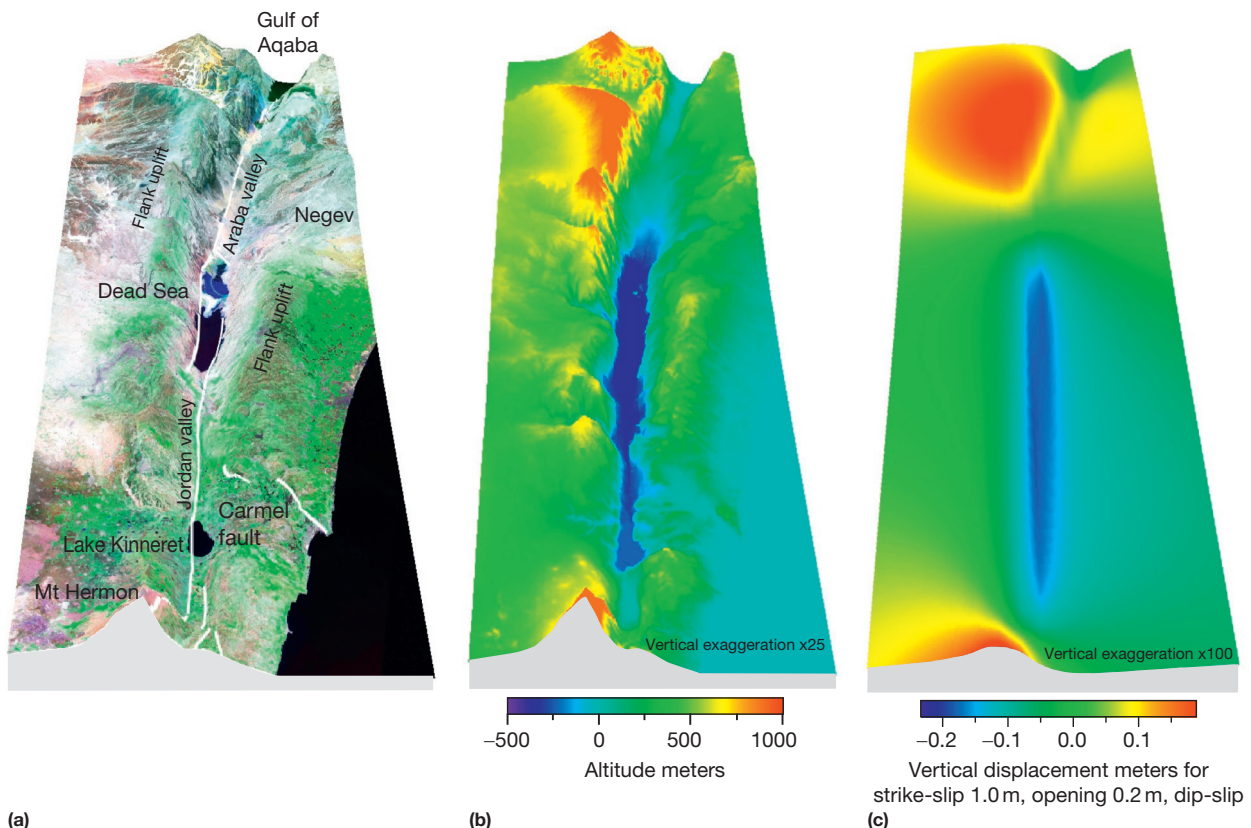


Figure 23 Topographic representations of the Dead Sea valleys (a) shows a Landsat Thematic Mapper image (band 2, red; 4, green; and 7, blue) draped over exaggerated digital elevation data (SRTM 3) to give a 3D effect. The vertical exaggeration is 25. The most prominent feature is the 11.5° change of valley strike occurring at the Dead Sea. While the valley is a clear feature, there are no clear normal faults marking the valley flanks (unlike Carmel Fault) such as in true rifts like Corinth or East Africa. (b) Shows a 3D image of the topography (SRTM3 data) colored by altitude. (c) Shows uplift and subsidence rates predicted by the model. Figure reproduced from Devès M, King GCP, Klinger Y, and Amotz A (2011) Localised and distributed deformation in the lithosphere: Modelling the Dead Sea region in 3 dimensions. *Earth and Planetary Science Letters* 308: 172.

commonly assumed the result of low friction on preexisting faults of varying orientation. Whatever the value of fault friction, multiple mechanisms are the only way to accommodate complex boundary conditions.

Although stresses associated with multimechanism faulting are inhomogeneous, the strain that is relieved by a collection of mechanisms can be simple (Amelung and King, 1997a,b). Figure 20(d) shows strain rosettes for the whole San Francisco Bay Area. Except for the largest magnitude ranges where there are insufficient events, the deformation due to all the small events summed in magnitude ranges is the same as that predicted by the overall plate motion and geodesy. The forms of the rosettes for subregions within the San Francisco Bay region are shown in Figure 22. These are consistent with geologic observations of the ongoing tectonics. For the Calaveras and Hayward faults, the strain rosettes can be explained by simple strike-slip faulting. Along the San Francisco peninsular and the Loma Prieta region, this is not the case; the strain conditions also require contractional

faulting. The subsiding Golden Gate region where the great 1906 earthquake is thought to have initiated is associated with substantial extension. This event could have started on a fault with a substantial normal component of slip and triggered by stresses very different from those that would be appropriate if the fault is represented by the average strike and mechanism of the San Andreas. This expands further on the remarks in Section 4.10.3.8 that suggest that resolving Coulomb stresses onto a plane determined from field measurements may not be appropriate.

Devès et al. (2011) have expanded on the kinematic approach modeling the Dead Sea valley system as an example. They use a distribution of dislocations to model the displacement field by matching the topography (Figure 23). This allows the strain field to be established that in turn allows the fault mechanisms to be predicted. Figure 24 shows that in the middle of the valley, colinear strike-slip mechanisms are predicted consistent with the kinematically stable direction followed by the main strike-slip Dead Sea fault. For the flanks of the valley both

Figure 22—cont'd 2 increase of fault dimensions. For creeping faults and volcanic or thermal spring regions, the moment release is the same for all bins. Insets show the equivalent b -values. The inset to (a) shows the observed scaling for regions in North California. The figures are simplified from Amelung and King (1997a,b). The rosettes are labeled with letters between A and F that correspond to magnitude bins A, 1.08–2.58; B, 2.58–3.33; C, 3.33–3.94; D, 3.94–4.54; E, 4.54–5.14; F, 5.14–5.75.

at the surface and at depth, stable faults cannot form requiring this deformation to be accommodated by multifault fragmentation. The modeling allows previously unexplained features of the valley to be accounted for. Although widely described as the Dead Sea Rift, the valley is not bounded by classic normal faults but by down warps composed of multiple and irregular faulting. The focal mechanisms also show a range of mechanisms. Both of these features can be explained by the distributed (process zone) deformation (Devès et al., 2011). There are other areas

such as the western Basin and Range in the United States where multiple faulting occurs, but which have not been studied in the way described.

The purpose of this chapter is to emphasize that while stress and stress transfer models can be powerful, they can capture only a part of how faults interact and suggest why (as noted in Section 4.10.3.8) in complex regions such as Loma Prieta Coulomb modeling of the aftershock sequence has not been successful.

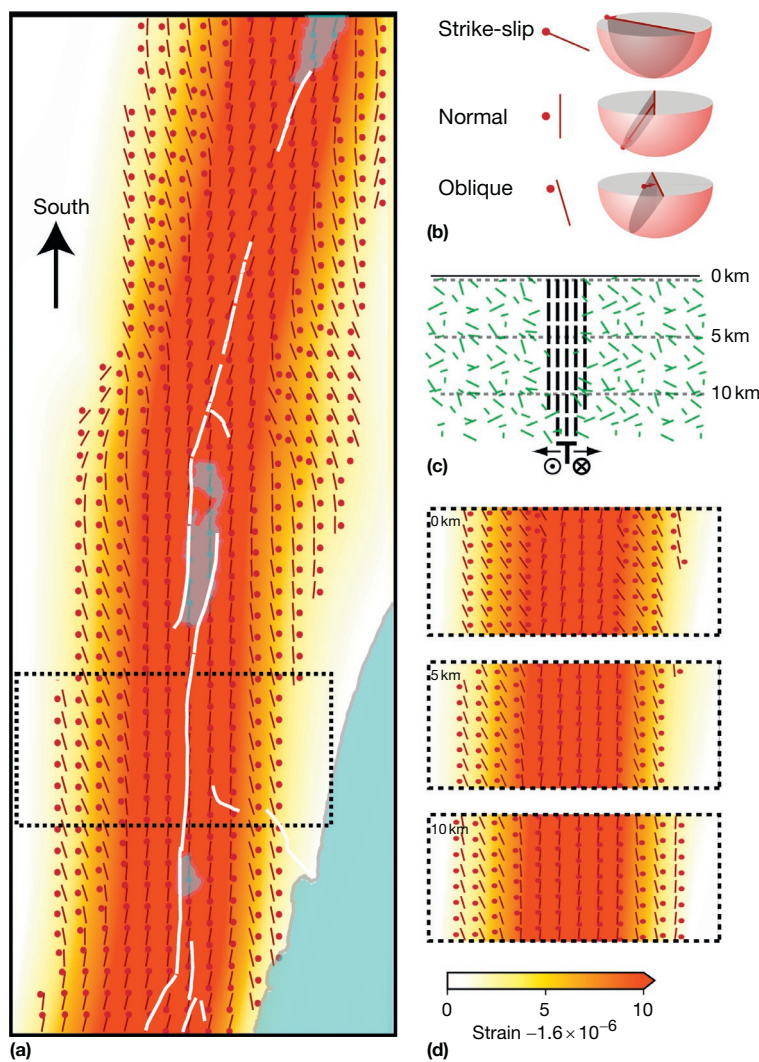


Figure 24 Predicted slip directions for the Jordan Rift. A regional vertical strain of -1.6×10^{-6} and a horizontal strain of 3.2×10^{-6} at -40° E and 0.0 at 50° W are applied. (a) Shows predicted directions for strike-slip, normal and oblique faults with left-lateral components at a depth of 5 km. The shading indicates strain (=geometric moment per unit volume). Note that only one of two possible dip directions is shown for normal faults. An inset, bottom right, shows the scale. Note that across the width of the rift the color scale is saturated. Only the strike-slip mechanisms near the center of the rift allow the creation of long kinematically stable faults parallel to the valley axis. These are consistent with the main active strike-slip faults. Many mechanisms on the flanks are normal with an extension direction $\sim 50^\circ$ E. Others have oblique mechanisms with varying ratios of normal to strike-slip components. Normal faulting parallel to the valley is not predicted. A change in the distribution of dislocation sources used to model deformation can slightly change the predicted slip directions but will not affect our main conclusions – flank deformation cannot localize on single throughgoing faults. (b) Shows the interpretation of the mechanisms shown in (a), (c) and (d). (b) Shows a schematic cross section indicating where strike-slip faulting can form (vertical lines) and where faulting cannot localize (green hatching) and indicates the depths at which (a) and (d) are calculated. (d) Shows predicted directions for different depths. Strike-slip mechanisms are predicted at all depth along the valley axis. Away from the axis, many mechanisms become oblique and are different at different depths. Normal faults parallel to the valley cannot develop. Since the predicted mechanisms are not kinematically stable, other faulting mechanisms must develop resulting in process zones of distributed deformation that creates the observed form of the valleys. Figure reproduced from Devès M, King GCP, Klinger Y, and Amotz A (2011) Localised and distributed deformation in the lithosphere: Modelling the Dead Sea region in 3 dimensions. *Earth and Planetary Science Letters* 308: 172.

4.10.6 Dynamic Triggering

This section concerns static stress triggering – its successes and failures. When discussing the latter, the possibility of events being triggered by large stresses associated with the passage of seismic waves must be considered. There is no doubt that dynamic triggering occurs; indeed, the propagation of rupture on a fault plane is a process of continuous triggering. At distances too great to result from static stress changes, events occur that are clearly related to the distant earthquake. The events in Alaska associated with 26 December 2004 Sumatra earthquake are a stunning example (West et al., 2005).

The dynamic triggering of events, however, cannot be explained by a failure occurring at a simple stress threshold as discussed in Section 4.10.2. Except near to the epicenter, the peak dynamic stresses associated with propagating seismic waves are much greater than those associated with the static stress change. Threshold triggering would result in every very big earthquake, triggering events all over the world. Because failure takes time (Section 4.10.4), this does not occur. Even large transient stresses are less important than sustained stresses.

If delayed failure suppresses dynamic triggering, why does it occur? At great distances, triggering is commonly associated with fluid processes, either water or magma, suggesting that special conditions are needed for it to occur (Hill et al., 2002). These are discussed in Chapter 4.11. Until the processes involved are better understood, events that appear in the negative lobes of static Coulomb stress change must be considered to be a possible consequence of dynamic stresses.

4.10.7 Conclusions

Relating the occurrence of one earthquake to another using changes of Coulomb stress is clearly successful. The distribution of aftershocks can be effectively explained in many cases. Interactions between large events have also been demonstrated and used to successfully predict destructive earthquakes (in Turkey and Sumatra). A problem with this approach is the modest length of most historical catalogs. This information can be recovered by geologic methods (fault geomorphology and trenching combined with steadily improved methods of dating), which will in due course greatly improve our understanding of earthquake hazard. Of equal importance, the concept of stress shadows can be used to suggest where destructive events are less likely to occur (Section 4.10.3.6). However, where these stress shadows fall along major faults, they do not last indefinitely. Adjacent loading over time restores the region to failure prior to the next substantial event. This is associated with increasing background activity in the region. Where it can be identified (Section 4.10.5.7), this provides a further approach to identifying the location of future damaging events. These results are of major social importance.

Stress interactions do not occur instantaneously – time is involved. The most successful approach to quantifying this invokes the concept of rate and state friction (Section 4.10.4.2). Following an abrupt stress increase, the rate at which small events occur increases. A combination of

Coulomb stress change and rate and state friction can explain both the distribution of aftershocks while the Omori law describes their rate of decay. The same approach can be adapted to predict an enhanced earthquake probability of a second event following a first. Such earthquake probability forecasts form the most effective way of communicating risk to government authorities, emergency services, and the general public, but it will be many years before the approach can be scientifically validated. Models that consider steadily increased loading as a result of viscous relaxation of the lower crust also aim to predict possibly times to future events (Nalbant and McCloskey, 2011; Parsons et al., 2008).

Despite the successes outlined, in many cases, earthquakes occur where they are not predicted by Coulomb stress changes alone. Many possible explanations have been discussed. Many draw on the fact that lithosphere is not a homogeneous elastic half-space, faults are not fully described by dislocation surfaces, and stress boundary conditions do not capture important features of finite deformation. Dynamic triggering can also explain features that cannot be explained by static stress models.

The problem with advancing our understanding of how earthquakes interact lies in finding data that can be interpreted unambiguously. At present, there are more models possible than data to distinguish between them. However, improvements in the data needed to understand lithospheric mechanics should come to our aid. For example, recent advances in our ability to map faults with the aid of satellite images and determine their rates with techniques such as cosmogenic dating. Space geodesy, both GPS and InSAR, is also placing constraints on the behavior of the lithosphere. In due course, these will allow a more of how and with what earthquakes interact. While we wait for the future, we are lucky that simple ideas work quite well and can certainly save lives.

Acknowledgment

The authors thank Renata Dmowska and Shinji Toda for helpful remarks. This is IPGP contribution number 2214 and INSU contribution number 396.

References

- Aki K and Richards P (1980) *Quantitative Seismology*. San Francisco, CA: W. H. Freeman and Co.
- Amelung F and King GCP (1997a) Large scale tectonic deformation inferred from small earthquakes. *Nature* 386: 702–705.
- Amelung F and King GCP (1997b) Earthquake scaling laws for creeping and non-creeping faults. *Earth and Planetary Science Letters* 24: 507–510.
- Ashby MF and Sammis CG (1990) The damage mechanics of brittle solids in compression. *Pure and Applied Geophysics* 133: 489–521.
- Bettinelli P, Avouac JP, Flouzat M, et al. (2008) Seasonal variations of seismicity and geodetic strain in the Himalaya induced by surface hydrology. *Earth and Planetary Science Letters* 266(3): 332–344.
- Bowman DD and Sammis C (2004) Intermittent criticality and the Gutenberg–Richter distribution. *Pure and Applied Geophysics* 161: 1945–1956.
- Chery J, Carretero S, and Ritz JF (2001) Postseismic stress transfer explains time clustering of large earthquakes in Mongolia. *Earth and Planetary Science Letters* 194(1): 277–286.
- Cocco M and Rice JR (2002) Pore pressure and poroelasticity effects in Coulomb stress analysis of earthquake interactions. *Journal of Geophysical Research* 107: 2030.

- Devès M, King GCP, Klinger Y, and Amotz A (2011) Localised and distributed deformation in the lithosphere: Modelling the Dead Sea region in 3 dimensions. *Earth and Planetary Science Letters* 308: 172.
- Devès MH, Tait S, King GCP, and Grandin R (in press) Strain heating in process zones; implications for metamorphism and partial melting of the lithosphere. *Earth and Planetary Science Letters*.
- Dieterich J (1994) A constitutive law for the rate of earthquake production and its application to earthquake clustering. *Journal of Geophysical Research* 99: 2601–2618.
- Ferguson CD, Klein W, and Rundle JB (1999) Spinodals, scaling, and ergodicity in a threshold model with long-range stress transfer. *Physical Review E* 60(2): 1359.
- Flerit F, Armijo R, King GCP, Meyer B, and Barka A (2003) Slip partitioning in the Sea of Marmara pull-apart determined from GPS velocity vectors. *Geophysical Journal International* 154(1): 1–7.
- Freed AM (2005) Earthquake triggering by static, dynamic, and postseismic stress transfer. *Annual Review of Earth and Planetary Sciences* 33: 335–367.
- Freed AM and Lin J (2001) Delayed triggering of the 1999 Hector Mine earthquake by viscoelastic stress transfer. *Nature* 411: 180–183.
- Gomberg J, Beeler NM, Blanpied ML, and Bodin P (1998) Earthquake triggering by transient and static deformations. *Journal of Geophysical Research: Solid Earth* (1978–2012) 103(B10): 24411–24426.
- Hardebeck JL, Feltzer KR, and Michael AJ (2008) Improved tests reveal that the accelerating moment release hypothesis is statistically insignificant. *Journal of Geophysical Research* 113: B08310. <http://dx.doi.org/10.1029/2007JB005410>.
- Harris RA (1998) Introduction to special section: Stress triggers, stress shadows, and implications for seismic hazard. *Journal of Geophysical Research* 103: 24347–24358.
- Harris RA and Simpson RW (1996) In the shadow of 1857 – The effect of the great Ft. Tejon earthquake on subsequent earthquakes in southern California. *Geophysical Research Letters* 23: 229–232.
- Helmstetter A and Sornette D (2002) Sub-critical and super-critical regimes in epidemic models of earthquake aftershocks. *Journal of Geophysical Research* 107: 2237.
- Helmstetter A, Sornette D, and Grasso JR (2003) Mainshocks are aftershocks of conditional foreshocks: How do foreshock statistical properties emerge from aftershock laws. *Journal of Geophysical Research: Solid Earth* (1978–2012) 108(B1).
- Hill DP (1977) A model for earthquake swarms. *Journal of Geophysical Research* 82: 1347–1352.
- Hill DP, Pollitz F, and Newhall C (2002) Earthquake–volcano interactions. *Physics Today* 55: 41–47.
- Hubert-Ferrari A, et al. (2000) Seismic hazard in the Marmara Sea following the 17 August 1999 Izmit earthquake. *Nature* 404: 269–272.
- Jackson JA, McKenzie DP, Priestley KF, and Emmerson B (2008) New views on the structure and rheology of the lithosphere. *Journal of the Geological Society* 165(2): 453–465.
- Jaumé SC and Sykes LR (1996) Evolution of moderate seismicity in the San Francisco Bay region, 1850 to 1993: Seismicity changes related to the occurrence of large and great earthquakes. *Journal of Geophysical Research* 101: 765–790.
- Jonsson S, Segall P, Pedersen R, and Björnsson G (2003) Post-earthquake ground movements correlated to pore-pressure transients. *Nature* 424(6945): 179–183.
- Kagan YY and Jackson DD (1991) Long-term earthquake clustering. *Geophysical Journal International* 104: 117–133.
- King GCP (1983) The accommodation of large strains in the upper lithosphere of the earth and other solids by self-similar fault system: The geometrical origin of b-value. *Pure and Applied Geophysics* 121: 761–815.
- King GCP (1986) Speculations on the geometry of the initiation and termination of earthquake rupture and the evolution of morphology and geological structures. *Pure and Applied Geophysics* 124: 567–585.
- King GCP and Bowman DD (2002) The evolution of regional seismicity between large earthquakes. *Journal of Geophysical Research* 107: 2354.
- King GCP and Cocco M (2000) Fault interaction by elastic stress changes: New clues from earthquake sequences. *Advances in Geophysics* 44: 1–38, Academic Press.
- King GC and Nabelek J (1985) The role of fault bends in faults in the initiation and termination of earthquake rupture. *Science* 238: 984–987.
- King GCP, Oppenheimer D, and Amelung F (1994a) Block versus continuum deformation in the western United States. *Earth and Planetary Science Letters* 128(3): 55–64.
- King GCP, Stein RS, and Lin J (1994b) Static stress changes and the triggering of earthquakes. *Bulletin of the Seismological Society of America* 84(3): 935–953.
- Lin J and Stein RS (2004) Stress triggering in thrust and subduction earthquakes and stress interaction between the southern San Andreas and nearby thrust and strike-slip faults. *Journal of Geophysical Research: Solid Earth* (1978–2012) 109(B2).
- Manighetti I, King GCP, and Sammis CG (2004) The role of off-fault damage in the evolution of normal faults. *Earth and Planetary Science Letters* 217(3): 399–408.
- Marsden D and Nalbant S (2005) Methods of measuring seismicity rate changes: A review of how the M 7.3 Landers earthquake affected the aftershock sequence of the M 6.1 Joshua Tree earthquake. *Pure and Applied Geophysics* 162: 1151–1185.
- McCloskey J, Nalbant SS, and Steacy S (2005) Indonesian earthquake: Earthquake risk from co-seismic stress. *Nature* 434(7031): 291.
- McKenzie DP and Morgan WJ (1969) Evolution of triple junctions. *Nature* 224: 125.
- Mignan A, King GCP, Bowman D, Lacassin R, and Dmowska R (2006) Seismic activity in the Sumatra–Java region prior to the December 26, 2004 ($M_w = 9.0–9.3$) and March 28, 2005 ($M_w = 8.7$) earthquakes. *Earth and Planetary Science Letters* 217: 339–408.
- Miller SA, Collettini C, Chiaraluce L, Cocco M, Barchi M, and Kaus BJ (2004) Aftershocks driven by a high-pressure CO_2 source at depth. *Nature* 427(6976): 724–727.
- Mindlin R (1936) Force at a point in the interior of a semi-infinite solid. *Physics* 195–202.
- Muir-Wood R and King GCP (1993) Hydrological signatures of earthquake strain. *Journal of Geophysical Research* 98: 22035–22068.
- Nalbant SS, Hubert A, and King GCP (1998) Stress coupling between earthquakes in northwest Turkey and the North Aegean Sea. *Journal of Geophysical Research* 103: 24469–24486.
- Nalbant SS and McCloskey J (2011) Stress evolution before and after the 2008 Wenchuan, China earthquake. *Earth and Planetary Science Letters* 307(2011): 222–232.
- Nalbant S, McCloskey J, Steacy S, and Barka AA (2002) Stress accumulation and increased seismic risk in eastern Turkey. *Earth and Planetary Science Letters* 195: 291–298.
- Noir J, Jacques E, Bekri S, Adler PM, Tappouer P, and King GCP (1997) Fluid flow triggered migration of events in the 1989 Dobi earthquake sequence of Central Afar. *Geophysical Research Letters* 24: 2335–2338.
- Nostro C, Stein RS, Cocco M, Belardinelli ME, and Marzocchi W (1998) Two-way coupling between Vesuvius eruptions and southern Apennine earthquakes, Italy, by elastic stress transfer. *Journal of Geophysical Research* 103: 24487–24504.
- Nur A and Booker JR (1972) Aftershocks caused by pore fluid flow. *Science* 175: 885.
- Ogata Y (1988) Statistical models for earthquake occurrence and residual analysis for point processes. *Journal of the American Statistical Association* 83: 9–27.
- Ogata Y (1989) Statistical model for standard seismicity and detection of anomalies by residual analysis. *Tectonophysics* 169: 159–174.
- Ogata Y (2004) Space–time model for regional seismicity and detection of crustal stress changes. *Journal of Geophysical Research* 109: B06308.
- Ogata Y, Jones LM, and Toda S (2003) When and where the aftershock activity was depressed: Contrasting decay patterns of the proximate large earthquakes in southern California. *Journal of Geophysical Research* 108(B6): 2318.
- Okada Y (1985) Surface deformation to shear and tensile faults in a half space. *Bulletin of the Seismological Society of America* 75: 1135–1154.
- Olami Z, Feder HJS, and Christensen K (1992) Self-organized criticality in a continuous, nonconservative cellular automaton modeling earthquakes. *Physical Review Letters* 68(8): 1244.
- Pacheco JF, Scholz CH, and Sykes LR (1992) Changes in frequency–size relationship from small to large earthquakes. *Nature* 355(6355): 71–73.
- Parsons T (2004) Recalculated probability of $M > 7$ earthquakes beneath the Sea of Marmara, Turkey. *Journal of Geophysical Research* 109: B05304. <http://dx.doi.org/10.1029/2003JB002667>.
- Parsons P, Ji C, and Kirby E (2008) Stress changes from the 2008 Wenchuan earthquake and increased hazard in the Sichuan basin. *Nature* 454: 509–510. <http://dx.doi.org/10.1038/nature07177>.
- Peltzer G, Rosen P, Rogez F, and Hudnut K (1998) Poro-elastic rebound along the Landers 1992 earthquake surface rupture. *Journal of Geophysical Research* 103: 30131–30145.
- Perfettini H and Avouac JP (2004) Stress transfer and strain rate variations during the seismic cycle. *Journal of Geophysical Research* 109: B06402.
- Pollitz F, Bakun WH, and Nyst M (2004) A physical model for strain accumulation in the San Francisco Bay region: Stress evolution since 1838. *Journal of Geophysical Research* 109: B11408. <http://dx.doi.org/10.1029/2004JB003003>.
- Pondard N, Armijo R, King GCP, Meyer B, and Flerit F (2007) Fault interaction in the Sea of Marmara pull-apart (North Anatolian Fault): Earthquake clustering and propagating sequences. *Geophysical Journal International* 171: 1185–1197. <http://dx.doi.org/10.1111/j.1365-246X.2007.03580>.
- Royden LH, Burchfiel BC, and van der Hilst RD (2008) The geological evolution of the Tibetan Plateau. *Science* 321: 1054. <http://dx.doi.org/10.1126/science.1155371>.

- Rundle JB, Klein W, Gross S, and Turcotte DL (1995) Boltzmann fluctuations in numerical simulations of nonequilibrium lattice threshold solids. *Physical Review Letters* 75: 1658–1661.
- Savage JC (1983) A dislocation model of strain accumulation and release at a subduction zone. *Journal of Geophysical Research* 105: 3095–3102.
- Scholz C (1990) *The Mechanics of Earthquakes and Faulting*. New York: Cambridge University Press, 439 pp.
- Scholz CH (1998) Earthquakes and friction laws. *Nature* 391: 37–42.
- Scholz CH (2002) *The Mechanics of Earthquakes and Faulting*. New York: Cambridge university press.
- Sibson RH (2002) Geology of the crustal earthquake source, edited, pp. 455–470. International Association for Seismology and Physics of the Earth's Interior, Committee on Education.
- Sornette D and Helmstetter A (2002) On the occurrence of finite-time-singularities in epidemic models of rupture, earthquakes and starquakes. *Physical Review Letters* 89: 158501.
- Steacy S, Gomberg J, and Cocco M (2005) Introduction to special section: Stress transfer, earthquake triggering, and time-dependent seismic hazard. *Journal of Geophysical Research: Solid Earth* (1978–2012) 110(B5).
- Stein RS (1999) The role of stress transfer in earthquake occurrence. *Nature* 402: 605–609.
- Stein R, Barka AA, and Dieterich JH (1997) Progressive failure on the North Anatolian fault since 1939 by earthquake stress triggering. *Geophysical Journal International* 128: 594–604.
- Stein RS, King GCP, and Jian L (1992) Change in failure stress on the southern San Andreas fault system caused by the 1992 Magnitude 7.4 Landers earthquake. *Science* 258: 1328–1332.
- Suppe J (1985) *Principals of Structural Geology*. Englewood Cliffs, NJ: Prentice-Hall, 537 pp.
- Toda S, Lin J, Meghraoui M, and Stein RS (2008) 12 May 2008 M = 7.9 Wenchuan, China, earthquake calculated to increase failure stress and seismicity rate on three major fault systems. *Geophysical Research Letters* 35: L17305. <http://dx.doi.org/10.1029/2008GL034903>.
- Toda S, Ross S, Stein RS, Gregory C, Beroza G, and David Marsan D (2012) Aftershocks halted by static stress shadows. *Nature Geoscience* 5: 410–413. <http://dx.doi.org/10.1038/ngeo1465>, Published online 6 May.
- Toda S, Stein RS, Richards-Dinger K, and Serkan B (2005) Forecasting the evolution of seismicity in southern California: Animations built on earthquake stress transfer. *Journal of Geophysical Research* 110(B5): B05S16.
- Volterra V (1907) Sur l'équilibre des corps élastiques multiplement connexes. *Annales scientifiques de l'École Normale Supérieure*. Paris 401–517.
- Walter TR and Amelung F (2007) Volcanic eruptions following $M \geq 9$ megathrust earthquakes: Implications for the Sumatra–Andaman volcanoes. *Geology* 35: 539–542.
- West M, Sánchez JJ, and McNutt SR (2005) Periodically triggered seismicity at Mount Wrangell, Alaska, after the Sumatra earthquake. *Science* 308(5725): 1144–1146.